REGULAR ARTICLE



WILEY

Check for updates

Cooperative acoustic navigation of underwater vehicles without a DVL utilizing a dynamic process model: Theory and field evaluation

Zachary J. Harris D | Louis L. Whitcomb

Department of Mechanical Engineering, Johns Hopkins University, Baltimore, Maryland, USA

Correspondence

Louis L. Whitcomb, Department of Mechanical Engineering, Johns Hopkins University, Baltimore, MD 21218, USA.

Email: Ilw@jhu.edu

Funding information

National Science Foundation, Grant/Award Numbers: 1319667, 1909182; Office of Naval Research, Grant/Award Number: National Defense Science and Engineering Fellowship

Abstract

This paper reports the theoretical development and at-sea field evaluation of a novel combined underwater acoustic communication and navigation system, known as cooperative acoustic navigation (CAN), for underwater vehicles (UVs) utilizing a second-order dynamic plant model of the submerged UVs. The present state-of-theart in CAN is to utilize one-way travel-time acoustic modem telemetry together with purely kinematic, constant-velocity plant process models. We term this approach CAN-KIN. At present, CAN-KIN is utilized with an on-board bottom-lock Doppler velocity log (DVL) providing frequent, high-accuracy velocity corrections. However, DVLs are relatively expensive, have significant power requirements, can be physically large, and have limited acoustic bottom-lock range, which restricts their use to a maximum of 25-420 m above the sea floor. In this study, we investigate the utility of a second-order dynamic UV plant process model in CAN of UVs equipped with an acoustic modem, attitude, and depth sensors, but lacking a DVL, and a surface ship equipped with an acoustic modem and global positioning system. We term CAN utilizing a dynamic model CAN-DYN. This paper reports results from at-sea field trials conducted in the Chesapeake Bay with the Johns Hopkins University Iver3 UV. These experimental results indicate the submerged UV position estimate from CAN-KIN is poor and even unstable in the absence of DVL velocity observations. These field experimental results also show that CAN-DYN performs well without a DVL. Our results suggest CAN-DYN without a DVL does not exhibit instability as does CAN-KIN without a DVL, performs similarly to CAN-KIN with a DVL, and outperforms DVL-based dead reckoning. Additionally, we report an experimental evaluation of the effect of adding (relative) velocity corrections in the form of acoustic range-rate observations to CAN utilizing a dynamic model without a DVL. We conclude that the addition of infrequent velocity observations, such as those provided by acoustic range rate, does not appear to improve the performance of CAN-DYN without a DVL.

KEYWORDS

cooperative acoustic navigation, dynamic process models for vehicle navigation, range-based navigation, underwater vehicle navigation

1 | INTRODUCTION

This paper addresses a cooperative acoustic navigation (CAN) problem arising in underwater vehicles (UVs) equipped with an acoustic modem, attitude, and depth sensors, but lacking a Doppler velocity log (DVL), and a surface ship equipped with an acoustic modem and global positioning system (GPS).

The case of UV navigation without a DVL sensor is relevant to low-cost UVs for which the cost, physical size, or power draw of a DVL may be prohibitive, and for missions in which the UV's altitude above the sea floor (or depth beneath overhead ice) exceeds the Doppler sonar's acoustic bottom-lock range—the most commonly used DVLs operate at frequencies of 300–1200 kHz with maximum bottom-lock acoustic range in sea water of approximately 25–420 m, respectively.

Navigation methods for UVs utilizing velocity signals (e.g., dead reckoning (DR) navigation or Doppler sonar navigation) or acceleration signals (e.g., inertial navigation) accumulate errors that grow unbounded with time or distance traveled and require independent observations of absolute position or velocity to correct the drift accumulated in the navigation estimate.

For land and air vehicle navigation, GPS provides an ideal independent source of position corrections for acceleration and velocity-based navigation systems (Chatfield, 1997), but GPS is unavailable to submerged UVs. Pressure depth sensor measurements are an excellent correction source for the depth (only) of velocity-based and acceleration-based position estimates. For submerged UVs (for which GPS is unavailable), few methods currently exist for absolute XY position corrections. The most common XY position correction methods are time-of-flight acoustic navigation systems, such as long-baseline (LBL) and ultra-short baseline (USBL) acoustic navigation (Hunt et al., 1974; Kinsey et al., 2006; Milne, 1983).

In this paper we address range-based one-way travel-time (OWTT) CAN in which a surface ship, equipped with a GPS and an underwater acoustic modem, transmits an acoustic data packet that encodes the precise time-of-launch (TOL) of the acoustic data packet (using a precision clock synchronized to GPS time) as well as the geodetic location and depth of the ships transducer at the TOL. When a submerged vehicle equipped with an underwater acoustic modem receives this data packet it timestamps the packet's time-ofarrival (TOA) (using an on-board precision clock synchronized to GPS time), and thus can compute the data packet's OWTT time-of-flight and, using the measured sound velocity of the water column, can compute the range from the ship transducer's location at TOL to the vehicle's transducer location at TOA. This range observation, together with signals from other sensors on-board the submerged vehicle such as a DVL, attitude and heading reference sensor (AHRS), and depth sensor, can be utilized to estimate the vehicle's geodetic position and velocity.

Range-only OWTT CAN uses ranges estimated from the acoustic time-of-flight between subsea nodes, for example, between two vehicles, or between a client vehicle and a server reference beacon of known (fixed or moving) location such as a surface ship. This method

provides both bounded-error position estimates and long range capabilities with reduced need for multiple costly fixed beacons, as is the case with most LBL systems. Unlike traditional two-way traveltime (TWTT) ranging, in which a single TWTT range can serve only one client, OWTT ranging offers the advantage that a single OWTT range can serve many clients. This method of combined acoustic navigation and communication is commonly called synchronous-clock CAN. For the duration of this paper, we define two important variants of the CAN state estimator: CAN utilizing a purely kinematic plant process model is called CAN-KIN, while CAN utilizing a dynamic plant process model is called CAN-DYN. Note that the process model for the CAN state estimator is independent of the sensor suite: both CAN-KIN and CAN-DYN can be utilized with or without a DVL.

To the best of our knowledge, this paper is the first detailed study of CAN utilizing a dynamic process model without a DVL, including an extensive at-sea field experimental evaluation and also the first reported evaluation of experimental acoustic range-rate data with the CAN-DYN state estimator. The present study complements and extends our previous studies on CAN (Harris & Whitcomb, 2015, 2016, 2018a, 2018b).

The remainder of this paper is organized as follows:

- 1. Section 2 reviews previously reported literature on range-based acoustic navigation of UVs.
- Section 3 reports the methodology behind the CAN state estimator, including the kinematic process model and the dynamic process model, and the observation models utilized by this algorithm.
- Section 4 briefly reviews the results of previously reported simulation results in the context of the CAN approaches reported herein.
- 4. Section 5 compares CAN-DYN without a DVL to CAN-KIN with and without a DVL on data obtained in at-sea experimental trials.
 - a. Section 5.1 describes the field experimental setup and procedures.
 - b. Section 5.2 reports a comparative performance analysis of CAN-DYN without a DVL and CAN-KIN with and without a DVL using acoustic range-only observations from three experimental autonomous underwater vehicle (AUV) dives.
 - i. Section 5.2.1 reports a comparison of the performance of CAN-DYN to CAN-KIN, both without a DVL.
 - ii. Section 5.2.2 reports a comparison of the performance of cooperative acoustic navigation utilizing a dynamic model (CAN-DYN) without a DVL to the "gold standard" of cooperative acoustic navigation utilizing a kinematic model (CAN-KIN) with a DVL.
 - iii. Section 5.2.3 reports an investigation of the repeatability of CAN-DYN without a DVL by comparing the navigation results for two different dives that utilized identical mission plans.
 - iv. Section 5.2.4 reports an investigation of the generalizability of CAN-DYN without a DVL by comparing the navigation

results for two different dives that utilized very different mission plans.

- v. Section 5.2.5 reports a comparison of XY position error magnitude of CAN-DYN without DVL navigation for three dives in comparison to conventional DR navigation, using the CAN-KIN with DVL as ground truth. Also reported is a comparison of the XY velocity error for the CAN-DYN state estimator without a DVL, computed as the difference between the CAN-DYN velocity estimate and the Iver3's RDI Explorer 600 kHz DVL.
- c. Section 5.3 reports result from Dive 55 comparing CAN-DYN utilizing acoustic range observations to CAN-DYN utilizing acoustic range-rate observations in addition to acoustic range observations.
- 5. Section 6 provides a summary and conclusion.

2 | LITERATURE REVIEW: UV NAVIGATION

Few techniques presently exist for reliable three-dimensional position sensing for UVs. Depth, altitude, heading, and roll/pitch attitude can all be instrumented with high bandwidth "strapdown" sensors mounted on the vehicle itself. XY position, in contrast, remains difficult to instrument and is normally measured acoustically. GPS cannot be used by submerged vehicles. Conventional long baseline (LBL) acoustic navigation systems require multiple fixed transponders—that is, fixed or moored on the sea floor (Hunt et al., 1974; Whitcomb et al., 1998), on the hull of a surface ship (Milne, 1983), or on sea-ice (Bellingham et al., 1994). With a maximum acoustic range of 5-10 km, fixed LBL networks can cover only limited mission areas. USBL navigation employs an array of transducers on a surface ship, and a transponder on a UV to compute the vehicle's 3-D position relative to the ship. The prevalence of LBL and USBL systems within the oceanographic community is due to a lacuna of other means for obtaining bounded-error XY position. Compact inertial navigation systems (INSs) have recently become commercially available (Gaiffe, 2002; Larsen, 2000a). INSs require additional position and velocity navigation sources to correct for accumulated errors. For a more exhaustive review of underwater navigation, see Kinsey et al. (2006).

Simultaneous localization and mapping (SLAM) seeks to exploit sensing capabilities of robots to correct for accumulated odometry error by localizing the robot with respect to landmarks in the environment (Moutarlier & Chatila, 1989; Smith et al., 1990). One SLAM methodology that has seen recent success in the near-seafloor underwater realm is to apply a view-based scan-matching approach, for example, Eustice et al. (2005); Eustice, Singh, & Leonard (2006); Eustice, Singh, Leonard, & Walter (2006); Fleischer (2000); Garcia et al. (2001); Roman (2005).

The development of underwater acoustic modems, however, has enabled underwater data telemetry at maximum ranges up to hundreds of kilometers (Catipovic & Freitag, 1990; Kilfoyls & Baggeroer, 2000; Partan et al., 2007; Singh et al., 1996; Webster et al., 2015). Maximum achievable acoustic telemetry range is strongly dependent on the carrier frequency, size, and mass of acoustic transducer and associated power electronics, and on the ambient acoustic conditions of the water column. Most smaller AUVs, such as the Iver3 AUV (L3 OceanServer), shown in Figure 1, utilize carrier frequencies in the 10–25 kHz ranges with maximum data telemetry range of 1–10 km. The propagation speed of acoustic telemetry in sea water about 1500 m/s, varying with temperature, salinity, and depth (Fofonoff & Millard, 1983). Acoustic data throughput varies widely with range, carrier frequency, acoustic bandwidth, encoding, and modulation method.

2.1 | Literature review of range-based underwater navigation

To the best of our knowledge, the earliest reported comprehensive study of underwater-vehicle navigation using acoustic ranging was

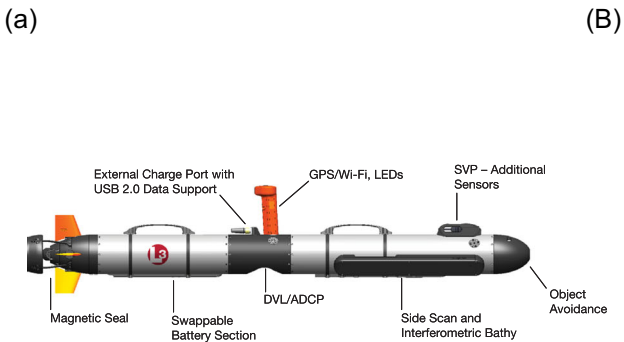




FIGURE 1 The Iver3 AUV is an underactuated AUV whose control authority is provided by the commanded rotational speed of its ducted propeller and commanded angles for the four red/yellow tail fins, all located at the stern of the vehicle. The 100 m depth-rated Iver3 AUV is one of several commercially available small AUVs designed for oceanographic survey operations including biological, physical-oceanographic, and bathymetric survey missions. (a) Iver3 general diagram (Image Credit: L3 OceanServer); (b) JHU Iver3-3026 is deployed from a small boat. AUV, autonomous underwater vehicle [Color figure can be viewed at wileyonlinelibrary.com]

reported by Hunt et al. (1974) in which they reported at-sea experimental evaluation of an acoustic approach to underwater-vehicle navigation in which a single UV could detect range from a set of fixed acoustic navigation transponders whose location was known a prioria method that has since been widely practiced and is now commonly known as LBL acoustic navigation. In Kinsey and Whitcomb (2004), the performance of bottom-lock Doppler navigation is evaluated with respect to LBL. In her 2006 MS thesis, LaPointe (2006) reports a single-beacon navigation approach in the form of a "virtual" LBL system (VLBL). The UV position is determined by advancing multiple ranges from a single transponder along the UV's DR track. The UV position is then triangulated using these successive ranges in a manner analogous to a "running fix" in surface ship navigation. Simulation results for the Woods Hole Autonomous Benthic Explorer (ABE) AUV are presented. Recent results on LBL have been reported, including Batista (2015), Batista et al. (2014), Jakuba et al. (2008).

Previous results by the authors and others (Bahr et al., 2009; Paull et al., 2014; Walls & Eustice, 2014; Webster et al., 2012, 2013) have shown the effectiveness of position corrections for Doppler and inertial navigation with range-only OWTT underwater navigation using ranges estimated from the acoustic time-of-flight of acoustic data packets between subsea nodes, for example, between two vehicles or between a vehicle and a reference beacon of known (fixed or moving) location.

Webster et al. report a system and at-sea evaluation for mesoscale cooperative navigation utilizing a 900 Hz carrier frequency to obtain OWTT acoustic ranges of up to 450 km. They report extensive field evaluation in which 11 acoustic beacons and four Seagliders AUVs were deployed in the Beaufort and northern Chukchi Seas (Webster et al., 2015).

Rypkema et al. report an inverted OWTT USBL system in which an AUV is equipped with an array transceiver that can receive acoustic transmissions from fixed acoustic beacon and calculate the azimuth, elevation, and range (in instrument coordinates) to the beacon which, together with vehicle attitude measurement from an inertial measurement unit (IMU), enables the calculation of vehicle position relative to the beacon with a single OWTT acoustic transmission (Rypkema et al., 2017).

Studies by the authors and others report the development and at-sea experimental evaluation of OWTT systems (including hardware and software) for the navigation of UVs using maximum-likelihood estimation (Eustice et al., 2011; Eustice, Whitcomb, Singh, & Grund, 2006), the extended Kalman filter (EKF) (Webster et al., 2012), and the extended information filter (EIF) (Webster et al., 2013, 2010).

Gallimore at al. report the development and at-sea evaluation of an OWTT system which the receiver performs carrier-phase tracking of a phase-shift keyed (PSK) acoustic signal to create fine-scale pseud-orange estimates in addition to, or in the absence of, OWTT TOAs (Gallimore et al., 2019).

Crasta et al. (2018) report a study of approaches to range-based CAN that support single or multiple UVs and single or multiple

beacon-equipped surface vehicles. Hung et al. (2020) report a study of range-based target navigation and pursuit employing a Bayesian estimation approach and model predictive control (MPC) approach for optimal control of "pursuit" vehicles in pursuit of moving "target" vehicles

Several authors have reported least-squares methods for single-beacon range-only navigation (Hartsfield, 2005; LaPointe, 2006; McPhail & Pebody, 2009; Scherbatyuk, 1995). Range-only target tracking has been addressed using EKFs and maximum-likelihood estimators (MLE) (Alleyne, 2000; Ristic et al., 2002; Song, 1999). The use of EKFs for homing and single-beacon navigation is reported in Baccou and Jouvencel (2002, 2003), Larsen (2000a, 2000b, 2002), Vaganay et al. (2000).

Recently, Claus et al. (2017) reported the comparison of a particle filter (PF) and centralized extended Kalman filter (CEKF) for OWTT navigation in post-processing on real-world data. The authors compare model-aided odometry, in the form of a water-velocity bias estimator, to DVL-aided odometry and conclude the PF slightly outperforms the CEKF. In both cases, a kinematic process model was used.

Most recently, Kepper et al. (2019) reported experimental results with OWTT acoustic navigation with a MEMS IMU and no DVL. The EKF utilizes a constant-acceleration process model with an accelerometer-bias model. The authors conclude the accuracy their approach is comparable to existing methods. We reported a preliminary numerical simulation study and pilot experimental evaluation with the Iver3 AUV for utilizing a dynamic UV plant model for CAN (Harris & Whitcomb, 2018a). The encouraging results of this preliminary paper are substantially extended herein.

Most previously approaches to UV navigation employ kinematic process models. One exception is Hegrenas et al. which reports the development and experimental evaluation of dynamic process model-aided INS for UVs (Hegrenas et al., 2008).

A number of studies have directly addressed the simultaneous estimation of UV state and ambient water current velocity (Claus et al., 2017; Crasta et al., 2013, 2014; Gadre & Stilwell, 2005a, 2005b; Gallimore et al., 2019; Hegrenas et al., 2008; Webster et al., 2015). Because the addition of estimation of ambient water current velocity is well understood, for simplifying of exposition in the present study we adopt the common approach that ambient water current is negligible, for example, Bahr et al. (2009), Moreno-Salinas et al. (2019), Rypkema et al. (2017).

2.1.1 | Literature review of observability of single-beacon range-based UV navigation

The observability of single-beacon range-based UV navigation has been studied extensively. Generally, previously reported studies have shown that the state of the submerged UV is observable provided there is sufficient richness and variability in the geometry of the slant ranges between the UV and a single (fixed or moving) acoustic beacon.

Scherbatyuk reported UV positioning method in the context of LBL acoustic positioning systems with on-board attitude sensor and velocity sensor based on least squares. Monte Carlo simulation results are presented to corroborate the analysis (Scherbatyuk, 1995).

Song reported necessary and sufficient conditions for local observability in the context of two-dimensional maneuvering with range measurements from a single beacon (Song, 1999). The approach taken in this paper utilizes the Fisher information matrix developed from the analytical treatment of system dynamics and noisy measurement equations established in a modified polar coordinate system. Numerical simulation results are presented to corroborate the analytical results.

Ristic et al. (2002) address the problem of target motion tracking from the range and range-rate measurements. A theoretical Cramer-Rao bound for the performance of an unbiased range-only tracking algorithm is derived, and three algorithms for target motion analysis are developed and compared to the theoretical performance bound. The three algorithms are the MLE, the EKF, and the regularized PF. Experimental validation of the theory is also presented.

Several studies addressed the observability of single-beacon range-only navigation with EKF estimation approaches (Gadre, 2007; Gadre & Stilwell, 2004, 2005a, 2005b; Lee et al., 2008). In Ross and Jouffroy (2005), the authors report a nonlinear observability analysis, identifying conditions under which the system is locally weakly observable. In Jouffroy and Reger (2006), the authors report employing nonlinear differential algebraic methods to derive conditions for observability.

Batista et al. (2010) address the observability for UVs navigation based on the range to a single beacon where the vehicle is equipped with an IMU and range measurements to a single source, in addition to angular velocity readings. The paper develops the necessary and sufficient conditions for observability for use in motion planning and control for an UV equipped with an IMU providing angular position and velocity measurements and range measurements to a single transducer. A Kalman filter (KF) is applied for body-frame state estimation, and simulation results are reported. In Batista et al. (2011), the authors extend their previous study (Batista et al., 2010), to address the necessary and sufficient conditions for observability of an mobile agent based on the based on the range to a single source, in addition to relative velocity readings (range-rate observations).

Crasta et al. (2013) address observability of an UV moving in two dimensions using acoustic range to a single beacon at a known location with a nonlinear, kinematic model. In the presence of known ocean currents, the system is found to be globally observable in the sense of Hermann and Krener (1977) for a constant relative course and constant (nonzero) relative course rate inputs. On the other hand, with unknown ocean currents the system fails to be locally weakly observable with constant relative course but the authors characterize the set of indistinguishable states from a given initial position and ocean current configuration and note that observability can be achieved with constant (nonzero) relative course rate in the presence of unknown, constant ocean currents. In Crasta et al. (2014), the authors extend the results of Crasta et al. (2013) to

address observability of an UV moving in three dimensions in the presence of ocean currents, under the assumption that the vehicle can only measure its acoustic range to a fixed transponder. A nonlinear, kinematic model is used and the UV can undergo any maneuvers that are completely parameterized by the body velocity, a constant flight path angle, and a constant yaw rate. In the presence of known, constant ocean currents, the 3D kinematic model of the AUV that corresponds to trajectories with nonzero flight path angle and yaw rate is observable. When the latter conditions fail, the authors give a complete characterization of the sets of states that are indistinguishable from a given initial state. In the case of unknown constant ocean currents, the model is shown to be locally weakly observable for nonzero yaw rate.

Quenzer and Morgansen (2014) explored control approaches to improve navigation performance of UVs deployed in survey missions. The authors propose methods for local observability measures to determine the immediate action (control) for a UV. Simulation studies show that one of the proposed methods has comparable or better performance than an existing maximum information gain method in a lawn mower style survey mission.

Arrichiello et al. (2013) address observability of single and multiple UVs navigation using acoustic range measurements with onboard sensors, including depth, velocity, and acceleration sensors. The paper examines the cases of a single UV ranging off a single transponder and multiple UV using inter-vehicle ranges. The paper shows that both the problems of absolute navigation of a single vehicle and the relative navigation of multiple vehicles may be treated using the same mathematical framework. Tailoring concepts of observability derived for nonlinear systems, the authors analyze how the performance in navigation depends on the types of motion imparted to the UV. They propose a well-defined observability metric and report simulation and experimental validation with an EKF state observer. They conclude that performance depends on the UV's motion.

Parlangeli and Indiveri (2014) address observability for single-beacon ranges with a kinematic UV model. Their paper extends previous results building on an augmented state technique allowing to reformulate the nonlinear observability problem in terms of a linear time varying (LTV) one. Globally unobservable motions are characterized in terms of initial conditions and commanded velocity signals. An underactuated model is considered, and a numerical simulation study is presented to demonstrate certain cases where the system is unobservable.

De Palma et al. (2017) address observability for the single beacon navigation problem of an UV using a nonlinear, kinematic "double integrator" model with acceleration as the model input and range to a stationary beacon as the output. The observability analysis addresses two complementary issues: the local weak observability for the nonlinear system, and, similar to Parlangeli and Indiveri (2014), the global observability for a LTV representation of the system derived through a state augmentation method. The proposed methods for observability analysis are discussed in different case studies (e.g., 2D/3D, absence/presence of current, and presence

of additional sensors like a DVL and a depth sensor). A numerical simulation study is presented to corroborate the analytical observability results.

Moreno-Salinas et al. (2019) report an exhaustive study of approaches to range-based CAN that support single or multiple UVs and single or multiple beacon-equipped surface vehicles, including addressing issues including observability and optimal sensor placement.

Additionally, several authors have addressed OWTT navigation of surface and UVs in a SLAM framework using distributed estimators (Bahr, 2009; Bahr & Leonard, 2006; Bahr et al., 2009; Bailey et al., 2011; Fallon et al., 2010).

2.2 | Literature review of UV navigation with acoustic range and range rate

To the best of our knowledge, the earliest study of underwater-vehicle navigation employing acoustic detection of *b*oth range and range rate was the 1978 study by Spindell et al. (1976), which extended the approach reported in Hunt et al. (1974) by reporting an experimental evaluation of an approach to underwater-vehicle navigation in which a single UV could detect both range and range rate from a set of fixed navigation whose location was known a priori.

Larsen studied employing acoustic range rate in addition to acoustic range for LBL navigation but did not report specific navigation algorithms for employing range rate nor any experimental evaluation (Larsen, 2000c, 2006). In Green and Scussel (2007), the authors report the notion of an underwater acoustic modem estimating and compensating for the Doppler shift of a received acoustic data packet transmission but do not address how a Doppler estimate might be used for navigation.

Ristic et al. (2002) and Batista et al. also investigated the use of range and range-rate for vehicle navigation, as described in Section 2.1.1.

In Bourgeois (2007), the author reported the experimental evaluation of algorithms for acoustically determining the *relative position* of two marine vehicles by employing measurement of acoustic range and acoustic range rate with specific focus on estimating relative positioning conditions, such as the closest-point-of-approach (CPA) of two vessels for the purpose of collision-avoidance.

In Harris and Whitcomb (2015), we investigated the effect of adding of acoustic range-rate measurements to acoustic range measurements in CAN using a kinematic model when the UV was equipped with a DVL. Using data obtained in numerical simulation, we concluded the addition of range-rate observations had minimal impact on the performance of CAN with a kinematic model when the UV was equipped with a DVL.

In Harris and Whitcomb (2016), we investigated the effect of adding of acoustic range-rate measurements to acoustic range measurements in CAN using a using a kinematic model when the UV not equipped with a DVL and was equipped with either (a) a high-accuracy fiber-optic gyroscope (FOG) IMU typically available on

high-end AUVs or (b) a low-end flux-gate compass and attitude sensor typically available on low-end AUVs. We concluded two things: First, for a UV equipped with a high-end fiber optic gyrocompass (FOG) attitude sensor, which is exceptionally accurate, acoustic range-rate observations in addition to acoustic range observations may offer modest improvements in the steady-state response and a significantly smaller error in the transient response of CEKF in CAN without a DVL compared to range-only navigation, especially in the situation when the acoustic range measurements are poor but the acoustic range-rate measurements are still valid. Second, a UV equipped with a low-end attitude sensor, which is typical on small, low-cost UVs such as the Iver3 AUV, we observed poor performance and instability of the CAN state estimator utilizing the kinematic model without a DVL when the UV was equipped with a low-cost attitude sensor such as the one available on the JHU Iver3 AUV

3 | CAN: METHODOLOGY

This section details the approach to OWTT CAN utilized to achieve the simulation and experimental results reported in Section 4 and Section 5, respectively.

Two formulations of CAN state estimators are presented in this section:

- Cooperative coustic navigation utilizing a kinematic model (CAN-KIN), described in Section 3.4, utilizes a nonlinear, kinematic model of the UV's motion with or without a DVL.
- Cooperative acoustic navigation utilizing a dynamic model (CAN-DYN), described in Section 3.5, utilizes a nonlinear, second-order dynamic model of the UV motion in place of velocity observations from a DVL.

3.1 | CAN formulation and implementation

We formulate the CAN state estimator as a discrete-time, delayed-state CEKF that uses a discrete process model to fuse depth and gyrocompass observations for the vehicle, GPS observations for the ship, and OWTT range and acoustic range-rate observations between the vehicle and the ship. Delayed states are required for causal processing of range measurements. The extended Kalman filter is an extension of the Kalman filter to nonlinear plants and observations by linearizing about the time-varying estimated state. For a full derivation and formulation of the EKF, see Bar-Shalom et al. (2001) and Thrun et al. (2005). The CEKF formulation of CAN assumes access to vehicle and ship sensor data simultaneously. Previous results have shown that the CEKF approach can be extended exactly to the decentralized extended information filter (DEIF) formulation of cooperative navigation (Webster et al., 2013).

The process model for the vehicle is linearized and discretized for use in the EKF using standard methods (Bar-Shalom et al., 2001).

Additionally, the reader is referred to Webster et al. (2012) for the subtleties of the modified process prediction, which occurs when the state augmentation is performed in concert with the process-prediction step.

3.2 | CAN state description

As is typical in CAN (Walls & Eustice, 2011; Webster et al., 2009, 2012), we define the state vector, x, as the composite of the current vehicle state, current ship state, and n delayed states. As mentioned above, delayed states are required for causal processing because the range measurement occurs between the ship at TOL and the vehicle at TOA. The state vector used in the CEKF for both CAN-KIN and CAN-DYN is

$$X = \begin{bmatrix} x_{v}^{\mathsf{T}} & x_{s}^{\mathsf{T}} & x_{v-1}^{\mathsf{T}} & x_{s-1}^{\mathsf{T}} & \dots & x_{v-n}^{\mathsf{T}} & x_{s-n}^{\mathsf{T}} \end{bmatrix}^{\mathsf{T}}, \tag{1}$$

where the current ship state $x_s \in \mathbb{R}^4$ is a 4-degree-of-freedom (DOF) vector containing the XY-position and respective velocity in world frame

$$x_{s} = \begin{bmatrix} x & y & \dot{x} & \dot{y} \end{bmatrix}^{T}, \tag{2}$$

and the current vehicle state $x_v \in \mathbb{R}^{12}$ is a 12-DOF vector containing the local-level pose and body-frame velocities

$$X_{V} = \begin{bmatrix} s^{T} & \varphi^{T} & \nu^{T} & \omega^{T} \end{bmatrix}^{T}, \tag{3}$$

$$s = \begin{bmatrix} x \\ y \\ z \end{bmatrix} \quad \varphi = \begin{bmatrix} \phi \\ \theta \\ \psi \end{bmatrix} \quad \nu = \begin{bmatrix} u \\ v \\ w \end{bmatrix} \quad \omega = \begin{bmatrix} p \\ q \\ r \end{bmatrix}, \tag{4}$$

where $s \in \mathbb{R}^3$ is the vehicle position and $\varphi \in \mathbb{R}^3$ is the vehicle attitude (in Euler angles) of the vehicle body-frame with respect to a local North-East-Down (NED) inertial frame of reference, $\nu \in \mathbb{R}^3$ is the body-frame linear velocity, and $\omega \in \mathbb{R}^3$ is the body-frame angular velocity. For convenience, we also define

$$\eta = \begin{vmatrix} s^T & \varphi^T \end{vmatrix}^T \mathbf{v} = \begin{vmatrix} v^T & \omega^T \end{vmatrix}^T,$$
(5)

where $\eta \in \mathbb{R}^6$ is the world NED-frame UV position and velocity vector and $v \in \mathbb{R}^6$ is the UV body-frame velocity vector.

3.3 | CAN ship process model

Because the ship has access to GPS position, we utilize a purely kinematic model for the ship in both CAN-KIN and CAN-DYN,

$$\dot{x}_{s} = \begin{bmatrix} 0 & \mathbb{I} \\ 0 & 0 \end{bmatrix} x_{s} + \begin{bmatrix} 0 \\ \mathbb{I} \end{bmatrix} w_{s}, \tag{6}$$

where $w_s \sim \mathcal{N}(0, Q_s) \in \mathbb{R}^2$ is the zero-mean Gaussian process noise with variance Q_s . Note that ship positions and velocities are represented in world-coordinates. In practice, we utilized process noise with a standard deviation of 0.1 m/s in x and y translation velocity and 1 degree/s in yaw rate.

3.4 | CAN-KIN: Kinematic UV process model

In CAN-KIN, we utilize a nonlinear, constant-velocity kinematic process model of the submerged UV, identical to the one reported in Webster et al. (2012).

The vehicle kinematics are

$$\dot{\eta} = K(\varphi)v, \tag{7}$$

where

$$K(\varphi) = \begin{bmatrix} R(\varphi) & 0 \\ 0 & L(\varphi) \end{bmatrix}$$
 (8)

is the kinematics matrix. $R(\varphi)$ is the transformation between inertial and body-frame linear velocities, and $L(\varphi)$ is the transformation between inertial and body-frame angular velocities. Explicitly,

$$R(\varphi) = R_z(\psi)^T R_v(\theta)^T R_x(\phi)^T, \tag{9}$$

where

$$R_{z}(\psi) = \begin{bmatrix} \cos(\psi) & \sin(\psi) & 0 \\ -\sin(\psi) & \cos(\psi) & 0 \\ 0 & 0 & 1 \end{bmatrix} \quad R_{y}(\theta) = \begin{bmatrix} \cos(\theta) & 0 & -\sin(\theta) \\ 0 & 1 & 0 \\ \sin(\theta) & 0 & \cos(\theta) \end{bmatrix}$$

$$R_{x}(\phi) = \begin{bmatrix} 1 & 0 & 0 \\ 0 & \cos(\phi) & \sin(\phi) \\ 0 & -\sin(\phi) & \cos(\phi) \end{bmatrix}, \tag{10}$$

and

$$\omega = e_1 \dot{\phi} + R_x(\phi) e_2 \dot{\theta} + R_x(\phi) R_y(\theta) \dot{\psi}$$
 (11)

$$= \begin{bmatrix} 1 & 0 & -\sin(\theta) \\ 0 & \cos(\theta) & \sin(\phi)\cos(\theta) \\ 0 & -\sin(\phi) & \cos(\phi)\cos(\theta) \end{bmatrix} \dot{\phi}, \tag{12}$$

where $e_1 = | \ 1 \ 0 \ 0 \ |^T \in \mathbb{R}^3, e_2 = | \ 0 \ 1 \ 0 \ |^T \in \mathbb{R}^3,$ and $e_3 = | \ 0 \ 0 \ 1 \ |^T \in \mathbb{R}^3$. Thus,

$$L(\varphi) = \begin{bmatrix} 1 & \sin(\phi)\tan(\theta) & \cos(\phi)\tan(\theta) \\ 0 & \cos(\phi) & -\sin(\phi) \\ 0 & \sin(\phi)\sec(\theta) & \cos(\phi)\sec(\theta) \end{bmatrix}. \tag{13}$$

We re-write (7) in state-space representation with the full 12 DOF vehicle state for use in the CEKF

$$\dot{\mathbf{x}}_{v} = \begin{bmatrix} 0 & 0 & R(\varphi) & 0 \\ 0 & 0 & 0 & L(\varphi) \\ 0 & 0 & 0 & 0 \\ 0 & 0 & 0 & 0 \end{bmatrix} \mathbf{x}_{v} + \begin{bmatrix} 0 & 0 \\ 0 & 0 \\ \mathbb{I} & 0 \\ 0 & \mathbb{I} \end{bmatrix} \mathbf{w}_{v}$$
(14)

where $w_v \sim \mathcal{N}(0, Q_v) \in \mathbb{R}^{12}$ is a vector of zero-mean Gaussian process noise with Q_v as the variance. UV positions are represented in inertial world coordinates, and UV velocities are represented in UV body coordinates. Empirically tuning the process-noise variance is a generally accepted practice for EKFs, and our best, most consistent results were achieved utilizing process noise with a standard deviation of 0.05 m/s^2 in translation velocity and 5 degrees/s^2 in angular rate. To ensure consistency when comparing results from the two

different process models, we used the same values for process noise in both CAN-KIN and CAN-DYN.

3.5 | CAN-DYN: Dynamic UV process model

CAN-DYN utilizes the second-order, nonlinear UV dynamics as the process model, as opposed to CAN-KIN which assumes a constant-velocity kinematic process model. The form of the second-order, nonlinear dynamics for an UV is well understood and has been since the 1950s (Society of Naval Architects and Marine Engineers (U.S.), Technical & Research Committee, & Hydrodynamics Subcommittee, 1950). Several sources develop the equations from first principles, including (Fossen, 1994; Paine, 2018) as

$$M\dot{v} + C(v)v + D(v)v + G(\varphi) = \tau(v, \xi),$$
 (15)

whose variables are defined in Section 3.2. We combine the kinematics (7) and the dynamics (15) to form the state-space process model for use in the CEKF as

$$\dot{x}_{v} = \begin{bmatrix} 0 & K(\varphi) \\ 0 & -M^{-1}(D(v) + C(v)) \end{bmatrix} x_{v} + \begin{vmatrix} 0 \\ M^{-1}(\tau(v, \xi) - \mathcal{G}(\varphi)) \end{vmatrix} + \begin{vmatrix} 0 \\ \parallel \end{vmatrix} w_{v},$$

$$(16)$$

where

- $K(\varphi): \mathbb{R}^3 \to \mathbb{R}^{6 \times 6}$ is the kinematics matrix, as defined in Section 3.4,
- $M \in \mathbb{R}^{6 \times 6}$ is the positive-definite symmetric (PDS) inertia matrix,
- $D(v): \mathbb{R}^6 \to \mathbb{R}^{6 \times 6}$ is the negative-definite symmetric (NDS) hydrodynamic drag matrix,
- $C(v): \mathbb{R}^6 \to \mathbb{R}^{6 \times 6}$ is the centripetal and Coriolis matrix,
- $\tau(\mathbf{v}, \xi) : \mathbb{R}^6 \times \mathbb{R}^{k+i} \to \mathbb{R}^6$ is the vector control forces and moments described in Section 3.5.1,
- $\mathcal{G}(\varphi): \mathbb{R}^3 \to \mathbb{R}^6$ is a vector of restoring forces and moments, and
- $w_v \sim \mathcal{N}(0, Q_v) \in \mathbb{R}^{12}$ is the zero-mean Gaussian process noise.

In practice, we achieved the best results with CAN-DYN when utilizing process noise with a standard deviation of 5 cm/s² for the translation velocity and 5 degrees/s² for the angular rate. The standard deviation in translation velocity is a full order of magnitude lower with the dynamic model than the kinematic model because, when the EKF does not have access to a DVL, the dynamic model is the main source of velocity information.

The inertia matrix, M, is a PDS matrix composed of the sum of the rigid-body inertia and added inertia, with scalar mass elements m_{ii} . It is convenient to write in block-matrix form, with block elements denoted $M_{ij} \in \mathbb{R}^{3\times3}$, because we use the block form to construct the Coriolis matrix.

$$M = M_{RB} + M_{A} = \begin{bmatrix} M_{11} & M_{12} \\ M_{21} & M_{22} \end{bmatrix}$$
 (17)

= diag(
$$[m_{11}, m_{22}, m_{33}, m_{44}, m_{55}, m_{66}]$$
). (18)

The drag matrix, D(v), is a negative-definite symmetric (NDS) matrix composed of the product of the quadratic hydrodynamic drag coefficients and their respective velocities

$$D(v) = diag(|v|) diag([d_{11}, d_{22}, d_{33}, d_{44}, d_{55}, d_{66}]).$$
 (19)

In constructing this drag matrix, we assume that there is no coupling between DOFs, that the vehicle is symmetric about the x, y, and z axes, and that linear drag terms have a small effect compared with their quadratic counterparts, which is discussed in Martin (2008). Note that the drag matrix inherently captures the effects of what many authors refer to as *body lift*. The diagonal terms d_{22} and d_{33} correspond to a body lift force in the y and z directions, respectively.

We parameterize the Coriolis matrix C(v) from M in (17) as

$$C(v) = \begin{bmatrix} 0 & -J(M_{11}v + M_{12}\omega) \\ -J(M_{11}v + M_{12}\omega) & -J(M_{21}v + M_{22}\omega) \end{bmatrix}$$
(20)

where J() is the skew-symmetric operator.

The buoyancy vector, $\mathcal{G}(\varphi)$, is defined as

$$G(\varphi) = \begin{vmatrix} R^{\mathsf{T}}(\varphi)e_3g_cg \\ -J(b)R^{\mathsf{T}}(\varphi)\rho\nabla g_c, \end{vmatrix}$$
 (21)

where $e_3 = |0\ 0\ 1|^T \in \mathbb{R}^3$, $g_c \in \mathbb{R}$ is the gravitational acceleration scalar with units of m/s^2 , $g_c g = (m - \rho \nabla) \in \mathbb{R}^3$ is the net buoyant force in Newtons, and $b \in \mathbb{R}^3$ is the vector from the center of buoyancy to the center of gravity in meters.

3.5.1 Dynamic UV process model control inputs

The CAN state estimator described and utilized herein requires the *value* of the control input signals, ξ , but it is completely agnostic to the specific control law utilized by the UV.

This section defines the nonlinear function, $\tau(v,\xi):\mathbb{R}^6\times\mathbb{R}^{k+i}\to\mathbb{R}^6$ to map the UV's control inputs, ξ , into a force-moment vector acting on the vehicle. We assume the vehicle is actuated with a combination of hydrodynamic control surfaces (e.g., fins) and propellers.

We define the following coordinate frames for each fin:

- V-Vehicle coordinate frame, centered at the UV's center of pressure (CP).
- F—Fin coordinate frame, centered at the fin CP when the fin is at commanded fin angle, δ, with the x-axis along the chord line of the fin and the y-axis pointing away from the center line of the vehicle.
- F_0 —Fin coordinate frame at $\delta = 0$.
- W—Flow coordinate frame, corresponding to the flow of water across the fin.

Note that the commanded fin angle, δ , is not the fin angle of attack to incident flow, α , so the F and W frames are generally not coincident. The position of the CP of the i^{th} fin in the vehicle frame is $p_i^V \in \mathbb{R}^3$ is the vector from the vehicle's center of gravity (CG) to the

CP of the i^{th} fin, and $\phi_i^V \in \mathbb{R}$ is the angular position of the i^{th} fin in the vehicle frame. We define the transformations between coordinate frames of each fin as

$$R_{iF}^{V} = R_{iF_0}^{V} R_{iF}^{F_0} \in \mathbb{R}^{3 \times 3},$$
 (22)

$$R_{iW}^{V} = R_{iF}^{V} R_{W}^{F} \in \mathbb{R}^{3 \times 3}, \tag{23}$$

where R_{iF}^V is the transformation from the fin frame to the vehicle frame and R_{iW}^V is the transformation from the flow frame to the vehicle frame. The individual transformations are defined as

$$R_{iF_0}^V = R_x \left(\phi_i^V \right), \tag{24}$$

$$R_{i\varepsilon}^{\mathsf{F}_0} = R_{\mathsf{v}}(\delta_i),\tag{25}$$

$$R_{iW}^F = R_v^T(\alpha_i), \tag{26}$$

where (24) is assumed because, for the vehicle used in the experimental results presented in this paper (Sections 4 and 5) and many other UVs, the x-axis of the fin frame aligns with the x-axis of the vehicle frame. The velocity of the *i*th fin through the water at the fin CP in vehicle coordinates is

$$\dot{p}_i^V = \nu + J(\omega) \ p_i^V, \tag{27}$$

and, thus, the velocity of the i^{th} fin in the fin frame F is

$$\dot{p}_i^F = R_{iF}^{\mathsf{TV}} \, \dot{p}_i^{\mathsf{V}}. \tag{28}$$

Assuming flow along the span of the airfoil does not affect the lift or drag, we use a projection matrix to find the flow along the x and z axes

$$\dot{p}_{xz_i}^F = \begin{bmatrix} 1 & 0 & 0 \\ 0 & 0 & 0 \\ 0 & 0 & 1 \end{bmatrix} \dot{p}_i^F, \tag{29}$$

from which we can find the angle of attack, α , as

$$\alpha_i = \operatorname{atan} 2(\dot{p}_{z_i}^F, \dot{p}_{x_i}^F), \tag{30}$$

where atan2 is the four-quadrant arc-tangent function. The lift and drag coefficients, $C_L(\alpha_i)$ and $C_D(\alpha_i)$, respectively, are a function of the angle of attack. We then compute the hydrodynamic lift and drag force

$$L(\alpha_i) = \frac{1}{2} \rho A C_D(\alpha_i) \| \dot{p}_{xz_i}^F \|^2, \tag{31}$$

$$D(\alpha_i) = \frac{1}{2} \rho A C_D(\alpha_i) \left\| \dot{p}_{xz_i}^F \right\|^2, \tag{32}$$

where A is the surface area of the fin. The force vector in the flow frame, W, is $f^W = -|D \ 0 \ L|^T$. Thus, the force vector from the *i*th fin in the vehicle frame is

$$f_i^{\mathsf{V}} = R_{i\mathsf{W}}^{\mathsf{V}} f_i^{\mathsf{W}}, \tag{33}$$

and the force and moment vector from is

$$\tau_i = \left| \begin{array}{c} f_i^{\mathsf{V}} \\ J(r_i^{\mathsf{V}}) f_i^{\mathsf{V}} \end{array} \right|. \tag{34}$$

The total force and moment vector on the vehicle with a total of N control surfaces is thus

$$\tau = \sum_{i}^{N} \tau_{i} + \left| \beta_{p} \omega_{p}^{2} O_{1 \times 5} \right|^{\mathsf{T}}, \tag{35}$$

where β_p is the propeller thrust coefficient such that

$$T = \beta_n \omega_n^2 \tag{36}$$

is the axial thrust of the propeller. This simplified thruster model is a reasonable assumption because we are modeling a ducted propeller with a high jet velocity compared to the advance velocity of the vehicle.

3.6 | CAN observation models

The range and range-rate observation models are nonlinear functions of the vehicle state at TOA and the ship state at TOL. Observation models of the additional sensors, including the DVL, GPS, depth sensor, and gyrocompass, are detailed in Webster (2010).

3.6.1 | CAN range observation model

As reported in (Webster et al., 2012), the range observation model can be written in matrix notation as

$$z_{rng} = (x^{T}A^{T}Ax)^{\frac{1}{2}} + v_{rng},$$
 (37)

where $v_{rng} \sim \mathcal{N}(0, R_{rng}) \in \mathbb{R}$ is zero-mean Gaussian noise and

$$A = \begin{bmatrix} -J_v & 0...0 & J_s & 0...0 \end{bmatrix}^T, \tag{38}$$

with J_v and J_s defined such that

$$J_{v}x_{v} = [x \ y \ z]^{T}, \tag{39}$$

$$J_s x_s = \begin{bmatrix} x_s & y_s & 0 \end{bmatrix}^T. \tag{40}$$

The measurement covariance, R_{rng} , is the variance of the range measurement. Table 1 shows the standard deviation of the range measurement gathered from experimental data.

The Jacobian of the range measurement with respect to the full state, *x*, is

$$H_{k} = \frac{\partial z_{mg}(x)}{\partial x} \bigg|_{x=\mu_{k|k-1}}$$

$$= \left(\mu_{k|k-1}^{\mathsf{T}} \mathsf{A}^{\mathsf{T}} \mathsf{A} \mu_{k|k-1}\right)^{-\frac{1}{2}} \mu_{k|k-1}^{\mathsf{T}} \mathsf{A}^{\mathsf{T}} \mathsf{A}. \tag{41}$$

3.6.2 | CAN range-rate observation model

As reported in Harris and Whitcomb (2016), the range-rate observation model is the time derivative of (37). Explicitly,

$$z_{rr} = (x^{T}A^{T}Ax)^{-\frac{1}{2}}x^{T}A^{T}\hat{A}x + v_{rr}, \tag{42}$$

where $v_{rr} \sim \mathcal{N}(0, R_{rr}) \in \mathbb{R}$ is zero-mean Gaussian noise and

$$\hat{A} = \begin{bmatrix} -\hat{J}_v & 0 \dots 0 & \hat{J}_s & 0 \dots 0 \end{bmatrix}^T, \tag{43}$$

TABLE 1 L3 OceanServer Iver3 AUV measurement sources and noise statistics

State	Measurement source	Measurement update rate or update period	Measurement SD
Range	WHOI Micromodem	5-15 s	1 m
Range-rate	WHOI Micromodem	5-15 s	0.1 m/s
Depth	OceanServer	4 Hz	10 cm
Heading, pitch, roll	OceanServer	4 Hz	1 °
Translation Velocity	600 kHz RDI DVL	5 Hz (when used)	1.4 cm/s (when used)

Note: These noise characteristics were determined from static tests of the sensors conducted by the authors, with the exception of the RDI DVL, which we obtained by interpolating data provided by the manufacturer for the UV's commanded speed in these experiments (1.3 m/s).

Abbreviations: AUV, autonomous underwater vehicle; DVL, Doppler velocity log.

with \hat{J}_v and \hat{J}_s defined such that

$$\hat{J}_{v} R(\varphi) x_{v} = |\dot{x} \quad \dot{y} \quad \dot{z}|^{T} \tag{44}$$

$$\hat{J}_{s} x_{s} = |\dot{x}_{s} \ \dot{y}_{s}| \ \mathbf{0}^{\mathsf{T}}. \tag{45}$$

The measurement covariance, R_{rr} , is the variance of the rangerate measurement. Table 1 shows the standard deviation of the range-rate measurement gathered from experimental data.

The Jacobian of (42) with respect to the full state, x, is

$$H_{k} = \frac{\partial z_{rr}(x)}{\partial x} \bigg|_{x=\mu_{k|k-1}}$$

$$= -\left(\mu_{k|k-1}^{\mathsf{T}} A^{\mathsf{T}} A \mu_{k|k-1}\right)^{-\frac{3}{2}} \left(\mu_{k|k-1}^{\mathsf{T}} A^{\mathsf{T}} A\right) \left(\mu_{k|k-1}^{\mathsf{T}} A^{\mathsf{T}} \hat{A} \mu_{k|k-1}\right)$$

$$+\left(\mu_{k|k-1}^{\mathsf{T}} A^{\mathsf{T}} A \mu_{k|k-1}\right)^{-\frac{1}{2}} \mu_{k|k-1}^{\mathsf{T}} (A^{\mathsf{T}} \hat{A} + \hat{A}^{\mathsf{T}} A), \tag{46}$$

where $\mu_{\mathbf{k}|\mathbf{k}-1}$ is the estimated mean of the world-frame position.

4 | SIMULATION RESULTS: CAN WITH A DYNAMIC UV PROCESS MODEL UTILIZING ACOUSTIC RANGE ONLY OBSERVATIONS

A challenging aspect of experimental field evaluation of UV navigation methods is that it is often difficult or impossible to know the "true"

vehicle state (position and velocity), and thus it is difficult or impossible to quantify precisely the "true error" of a proposed navigation method. In Section 5, we report at-sea field experimental trials, in which we necessarily use indirect methods to evaluate navigation performance. In numerical simulation studies, however, it is always possible to know the "true" vehicle state, and thus possible to quantify precisely the "true error" of a proposed navigation method. We reported a simulation study in our previous work (Harris & Whitcomb, 2018a), in which we concluded that CAN-DYN without a DVL vastly outperformed CAN-KIN without a DVL and performed approximately as well as CAN-KIN with a DVL. In that preliminary study, we also reported that the simulation results corroborated the results from a preliminary pilot field experiment conducted in the Chesapeake Bay. Indeed, the simulation results are quite similar to the results from field experiments and show that the navigation error for both CAN-DYN without a DVL and CAN-KIN with a DVL is on the order of meters. Our main concern, however, with the simulation study is that the dynamic model used to compute the "true" state was the same as the dynamic model used as the process model. In reality, a UV operating in the real world will experience exogenous forces unmodeled dynamics not perfectly modeled by 15. Thus, in the present study, we seek to corroborate our previous simulation results with experimental results from at-sea field testing in Section 5 below.

TABLE 2 Acoustic modem time division multiple access (TDMA) cycle

Time	Action	Comment	Packet type
00 s	Begin of TDMA cycle		
00 s	OWTT data packet + range uplink AUV status packet to Ship	AUV status uplink. Not used for CAN	64 byte, PSK
05 s	OWTT data packet+range downlink of CAN data packet from Ship to AUV	Used for CAN	64 byte, PSK
10 s	OWTT data packet + range downlink of CAN data packet from Ship to AUV	Used for CAN	64 byte, PSK
15 s	OWTT data packet+range downlink of CAN data packet from Ship to AUV	Used for CAN	64 byte, PSK
20 s	TWTT range ping AUV to Ship, with Ship to AUV reply	TWTT range. Not used for CAN	32 bit, PSK
25 s	Reserved for commands sent to AUV from Ship		
30 s	End of TDMA cycle	Begin next TDMA cycle	

Abbreviations: AUV, autonomous underwater vehicle; CAN, cooperative acoustic navigation; OWTT, one-way travel-time; TWTT, two-way travel time.

TABLE 3 Sensors used for comparative experimental evaluations

Sections	Comparision	Range	DVL	Range-rate	Depth	AHRS	Ship GPS
5.2.1	CAN-DYN without DVL to CAN-KIN without DVL	KIN DYN			KIN DYN	KIN DYN	KIN DYN
5.2.2	CAN-DYN without DVL to CAN-KIN with DVL	KIN DYN	KIN		KIN DYN	KIN DYN	KIN DYN
5.2.3	CAN-DYN without DVL repeatability	DYN			DYN	DYN	DYN
5.2.4	CAN-DYN without DVL generalizability	DYN			DYN	DYN	DYN
5.2.5	CAN-DYN without DVL vs. DR	DYN DR			DYN DR	DYN DR	DYN DR
5.3	CAN-DYN, no DVL, with and without range-rate	DYN		DYN with and without	DYN	DYN	DYN

Abbreviations: AHRS, attitude and heading reference sensor; CAN, cooperative acoustic navigation; DVL, Doppler velocity log; GPS, global positioning system.

5 | EXPERIMENTAL RESULTS: CAN WITH A DYNAMIC UV PROCESS MODEL

This section reports the results of three at-sea field trials to conduct a comparative experimental evaluation of the reported CAN state estimators on experimental data obtained with JHU's Iver3 AUV (L3 OceanServer), shown in Figure 1, in the Chesapeake Bay. Data are reported for three dives with the Iver3 AUV described in Section 5.1.1: Dive 55, 57, and 60. This section is organized as follows:

- Section 5.1 describes the field experimental setup and procedures.
- Section 5.2 reports a comparative performance analysis of CAN-DYN without a DVL and CAN-KIN with and without a DVL using acoustic range-only observations from three experimental AUV dives.
 - a. Section 5.2.1 reports a comparison of the performance of CAN-DYN to CAN-KIN, both without a DVL.
 - b. Section 5.2.2 reports a comparison of the performance of CAN-DYN without a DVL to the "gold standard" of CAN-KIN with a DVL.
 - c. Section 5.2.3 reports an investigation of the repeatability of CAN-DYN without a DVL by comparing the navigation results for two different dives that utilized identical mission plans.
 - d. Section 5.2.4 reports an investigation of the generalizability of CAN-DYN without a DVL by comparing the navigation results for two different dives that utilized very different mission plans.
 - e. Section 5.2.5 reports a comparison of XY position error magnitude of CAN-DYN without DVL navigation for three dives in comparison to conventional DR navigation, using the CAN-KIN with DVL as ground truth. Also reported is a comparison of the XY velocity error for the CAN-DYN state estimator without a DVL, computed as the difference between the CAN-DYN velocity estimate and the Iver3's RDI Explorer 600 kHz DVL.
- Section 5.3 reports results from Dive 55 comparing CAN-DYN utilizing acoustic range observations to CAN-DYN utilizing

acoustic range-rate observations in addition to acoustic range observations.

5.1 | CAN experimental setup and procedure

We conducted field trials with a surface ship and JHU's Iver3 AUV (L3-Harris OceanServer) (L3 OceanServer, 2016) in the Chesapeake Bay, MD, USA. The AUV is an under-actuated AUV equipped with a 600 kHz Phased Array RDI Explorer DVL (Teledyne RD Instruments) (Teledyne, 2017), and an OceanServer OS5000 digital compass (L3-Harris OceanServer) which measures magnetic heading, pitch, roll, and pressure depth (L3 OceanServer, 2015). Figure 1 shows JHU Iver3 AUV during the vehicle tests. Table 1 lists the noise characteristics of the sensors on board the JHU Iver3 AUV. These noise characteristics were determined from static tests of the sensors conducted by the authors, with the exception of the RDI DVL, which we obtained by interpolating data provided by the manufacturer for the UV's commanded speed in these experiments (1.3 m/s). While submerged on these dives the DVL experienced bottom-lock beam ranges of between 2 and 8 m with a typical DVL update period of 0.2 s or less.

The real-time geodetic location of the surface ship's modem transducer was instrumented with a GPS unit located vertically above the acoustic modem's transducer. This GPS unit was a Navisys GR-701W u-blox-7 (NaviSys Technology Corp.), which reported fixes at 1s intervals with a reported horizontal dilution of precision (HDOP) values with a mean just under 1.0.

For the control inputs of propeller speed and fin angle to the model described in Section 3.5.1, we utilized the values commanded and logged by the Iver3's control system, provided by the vehicle manufacturer.

The surface ship and the Iver3 AUV were each equipped with 25 kHz WHOI Micromodem IIs (Gallimore et al., 2010; Singh et al., 2006), each equipped with precision Microsemi Quantum chip-scale atomic clocks (Microsemi Corporation) and precision-timing GPS units to synchronize the clocks to GPS UTC time. The acoustic modems on the Iver3 and the ship were programmed to repeat the 30-second time-division multiple access (TDMA) acoustic telemetry

cycle listed in Table 2. The TDMA cycle given in Table 2 started precisely at the top and the bottom of every UTC minute to coordinate when the AUV or ship modem transmitted. The Micromodem IIs were configured for synchronous navigation (parameter SNV = 1), precision TOA reporting (parameter TOA = 1), and Doppler range-rate reporting (parameter DOP = 1) which reports range-rate averaged over the data packet. Both ship and AUV modems had their TDMA cycles controlled by a modem driver process running on a host Linux CPU. The ship and AUV host CPUs and modems were all provided with precision-clock signals to synchronize their clocks to GPS UTC time (even when submerged, in the case of the AUV).

The senors employed for the comparative experimental CAN evaluations are given in Table 3.

For CAN data packets with data transmission and simultaneous OWTT ranging, we employed the WHOI Micromodem II configured for Band 2 (25 kHz carrier frequency) and single-frame 64-byte phase-shift keying (PSK) data packets (Packet type = 1), no acknowledgment minipackets (ACK = 0), MST parameter set to (MST = 1), with a data packet duration of 1.9 s. We had good acoustic conditions and the packet transmission success was excellent. Each CAN OWTT downlink packet was encoded with the geodetic coordinates of the ship's modem transducer at the TOL of the OWTT downlink transmission, the exact TOL of the OWTT downlink transmission, and status information on the precision clock status of the ship's modem. When the AUV modem received a downlink packet it timestamped the TOA of the OWTT downlink transmission, and with the data encoded in the packet can compute time-of-flight with sub-millisecond accuracy.

In addition to the CAN OWTT downlink packets, each TDMA cycle contained one uplink data packet from AUV to ship containing vehicle status information, and one conventional TWTT ranging ping initiated by the AUV.

5.1.1 | Dive mission plans

Herein we report results from three dives with the Iver3 AUV on December 11, 2017 with the following mission plans:

- In Dive 55 and 60, the Iver3 AUV was programmed to run identical rectangular survey pattern with six 300 m legs spaced 50 m apart at a constant depth of 2.5 m traveling at an advance velocity of 1.3 m/s. This constant-depth mission is typical for multi-beam sonar bathymetric survey missions.
- In Dive 57, the Iver3 AUV was programmed to run a rectangular survey pattern with four 300 m legs spaced 50 m apart at an advance velocity of 1.3 m/s while undulating from 1 to 5 m depth at with a maximum pitch angle of 20 degrees. This undulating-depth mission is typical for physical oceanographic conductivity, temperature, and depth (CTD) surveys, and for biological oceanographic plankton surveys. We include Dive 57 to evaluate whether the results from constant-depth Dives 55 and 60 generalize to missions with highly time-varying depth.

5.1.2 | CAN state estimator initialization

During these experiments, the UV position in the CAN state was initialized to the last valid GPS fix of the Iver3 AUV before it submerged, and the UV surge velocity was initialized to the DVL reading at that same time or, in the case of no DVL, the Iver3 commanded forward speed. The sway and heave velocities were initialized to zero.

5.1.3 | Real-time vehicle control setup

This paper focuses purely on the navigation problem. In these experiments, the JHU Iver3 AUV ran pre-programmed missions, detailed in Section 5.1.1, in the Chesapeake Bay utilizing the Iver3's waypoint-based mission planner, navigation system (likely DR), and control system all supplied by the manufacturer. The data collected on each dive were post-processed utilizing the CAN algorithm variants: CAN-DYN, CAN-KIN without a DVL, and the previous "gold standard" of CAN-KIN with a DVL. Thus, the Iver3 AUV did not utilize the output of the various CAN state estimates as an input to the Iver3's control system in real time. For this reason, the position estimate from any of the CAN state estimators may diverge from the desired trackline as the DR error grows, and the distance from the Iver's desired waypoint trackline shown in the figures below is not the navigation error.

We address the feasibility of combined control and navigation without a DVL using CAN-DYN in a previously reported simulation study (Harris & Whitcomb, 2018b), in which we report that closed-loop navigation and navigation is feasible and stable with CAN-DYN without a DVL using an linear quadratic regulator (LQR) controller and the CEKF described above.

5.1.4 | Estimation of experimental navigation errors

Because this is a field experiment with a submerged UV (GPS does not work when the UV is submerged), we do not have access to the true vehicle positions and are therefore unable to compare the navigation error—that is, the difference between the true XY position of the vehicle and the state estimate—of CAN-KIN to CAN-DYN. Instead we utilize the previous "gold standard" of CAN-KIN with a DVL as the true vehicle position.

Comparing CAN-DYN without a DVL to CAN-KIN with a DVL is really a comparison of the velocity estimate from the dynamic model to the velocity measured by the DVL. Because it is unlikely the dynamic model could estimate the UV's velocity more accurately than it would be measured by a DVL, we have no expectation that CAN-DYN would outperform CAN-KIN with a DVL, except in cases where the DVL fails, for example, when the range to the sea floor is beyond the bottom-lock range of the DVL.

A discussion on the navigational accuracy of CAN-KIN with a DVL, including comparisons with other methods of acoustic navigation, such as LBL, may be found in Webster et al. (2012).

The magnitude of the difference in the XY position estimate of CAN-DYN and CAN-KIN with a DVL is shown in Section 5.2.5 for all three dives. For the remainder of this paper, this difference will be referred to as the "navigation error."

5.1.5 | Dynamic model parameters

The parameters for the dynamic model were empirically tuned to match the translation velocity predicted by the model to the translation velocities reported by the DVL in surge and sway. A principled method for estimating plant-model parameters and control-actuator parameters for torpedo-shaped, underactuated UVs is the subject of ongoing and future research; a preliminary approach was reported by the authors in Harris et al. (2018). In this paper, the model parameters were empirically tuned for Dive 55, and the results reported for Dive 60 and Dive 57 utilize the same dynamic plant-model parameters that were tuned for Dive 55.

5.2 | Experimental results: CAN-DYN utilizing acoustic range only observations

This section reports experimental results for CAN comparing the navigation performance of the CAN-DYN state estimator without a DVL to the CAN-KIN state estimator with and without a DVL.

5.2.1 | Experimental results: Comparison of CAN-DYN without a DVL to CAN-KIN without a DVL

This section reports a comparison of the performance of CAN-DYN to CAN-KIN, both without a DVL, utilizing experimental data collected from Iver3 Dive 55.

Figure 2 shows the mean of the CAN-estimated UV and ship XY position estimates for Iver3 Dive 55. Figure 2a shows the CAN-KIN state estimate without a DVL and Figure 2b shows the CAN-DYN state estimate without a DVL. The dashed blue line is the CAN position estimate of the Iver3 AUV, the black dots are the CAN position estimate of the surface ship, and the red triangle is the first GPS fix after the UV surfaced. The EKF solution for the ship position is similar to the GPS track of the ship position, with minimal smoothing dependent on the ship process noise. The pink ellipses in Figure 2b are 3σ ellipses from the CAN-DYN state estimator plotted at every acoustic update. 3σ ellipses for CAN-KIN without a DVL are omitted from Figure 2a because the position covariance from the CAN-KIN state estimator without a DVL is so large that the plot is unreadable. As noted in Section 5.1.3, the Iver3 AUV did not use the position estimate from the CAN state estimator as the position input to the control system during these experiments, and the distance from the trackline is likely the difference between the DR and CAN navigation solutions rather than the CAN navigational error.

Figure 2a shows the UV position estimate from CAN-KIN without a DVL is extremely poor and quickly exhibits instability, and Figure 2b illustrates that the CAN-DYN state estimator performs well and offers a stable solution without a DVL. We spent a considerable amount of time tuning the process noise for CAN-KIN to achieve better results, and these results are representative of the

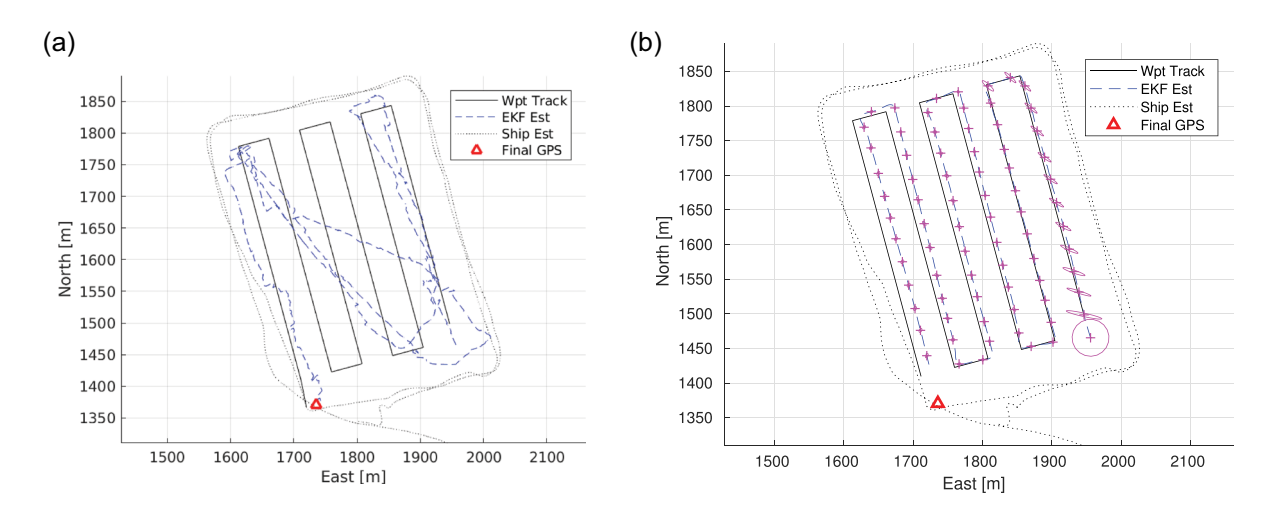


FIGURE 2 Ship and vehicle XY position estimate using (a) CAN-KIN without a DVL and (b) CAN-DYN without a DVL on experimental data collected with the JHU Iver3 AUV in the Chesapeake Bay. The dotted black line is the CAN ship position estimate, and the dashed blue line is the CAN UV position estimate, computed in post-processing. The first valid GPS fix upon surfacing is plotted as a red triangle. The pink ellipses are 3σ ellipses from the CAN state estimator plotted at every acoustic update. This figure shows that for a UV equipped with sensors typical of low-cost UVs, such as the JHU Iver3 AUV, CAN-DYN without a DVL offers a stable position estimate, in contrast to CAN-KIN without a DVL. AUV, autonomous underwater vehicle; CAN, cooperative acoustic navigation; DVL, Doppler velocity log; GPS, global positioning system [Color figure can be viewed at wileyonlinelibrary.com]

best we were able to achieve with the sensor characteristics detailed in Table 1.

The magnitude of the difference in the position estimate of CAN-DYN and CAN-KIN with a DVL is shown in Figure 12 in Section 5.2.5 for all three dives.

Because CAN provides infrequent position corrections in the form of an acoustic time-of-flight (TOF), which is converted into a range using the speed of sound in water, it is vitally important that the state estimator accurately estimate the submerged UV's velocity between acoustic position corrections. This velocity estimate is integrated continuously to propagate the position estimate between acoustic position corrections. The velocity estimates from CAN-DYN and CAN-KIN without a DVL provides additional insight into the performance gap between the two state estimators in the absence of velocity measurements from a DVL.

Figure 3 shows the velocity estimate from CAN-DYN (without a DVL) for Dive 55, and Figure 4 shows the velocity estimate from CAN-KIN without a DVL for Dive 55. We did not include the velocity plots for CAN-KIN with a DVL because the velocity estimate tracks the DVL measurements exactly, with some amount of smoothing dependent on the process noise. In both figures, the red dots are the Iver3 AUV 600 kHz RDI DVL measurements, and the dashed blue line is the mean of the CAN state estimator's velocity estimate. Note that the scale of the vertical axis is significantly larger on Figure 4 than Figure 3, and the red dots of the DVL measurements are the same signal on both plots. The velocity transient spikes occur when the vehicle is turning: the surge velocity drops because the high fin angle of the Iver3's vertical fins increases the overall drag on the Iver3; the sway velocity increases when the Iver3 experiences

sideslip during turns because, although the Iver3 is underactuated, it is not a nonholonomic system.

As shown in Figure 3, the velocity estimate from the CAN-DYN state estimator is quite accurate in both surge and sway, even in turns when the UV experiences a drop in surge velocity from fin drag and an increase in sway velocity. This figure illustrates the performance of CAN-DYN at modeling the UV's velocity. Accurate velocity estimation is crucial to accurate position estimation because CAN provides infrequent position updates; in the absence of DVL measurements, the velocity estimate depends entirely on the model.

In contrast, Figure 4 shows the constant-velocity kinematic model typically used in CAN fails dramatically in the absence of a DVL. A constant-velocity assumption is reasonable when the vehicle has access to frequent, high-accuracy velocity observations, such as when the vehicle is equipped with a DVL, because the velocity estimate experiences minimal drift between velocity corrections. However, the velocity estimate from a constant-velocity model with infrequent position corrections and no velocity corrections can drift substantially between position corrections.

We did not include velocity plots for the heave (Z) DOF because the Iver3 AUV is equipped with a pressure depth sensor, as noted in Table 1, which provides depth measurements at $4\,\mathrm{Hz}$ with a standard deviation of $10\,\mathrm{cm}$.

Given the infrequency of position updates, we believe the performance of the position estimate is driven primarily by the ability of the CAN state estimator to estimate the UV's motion. Thus, we conclude that the poor performance and instability of the position estimate from CAN-KIN without a DVL is caused by the inability of a

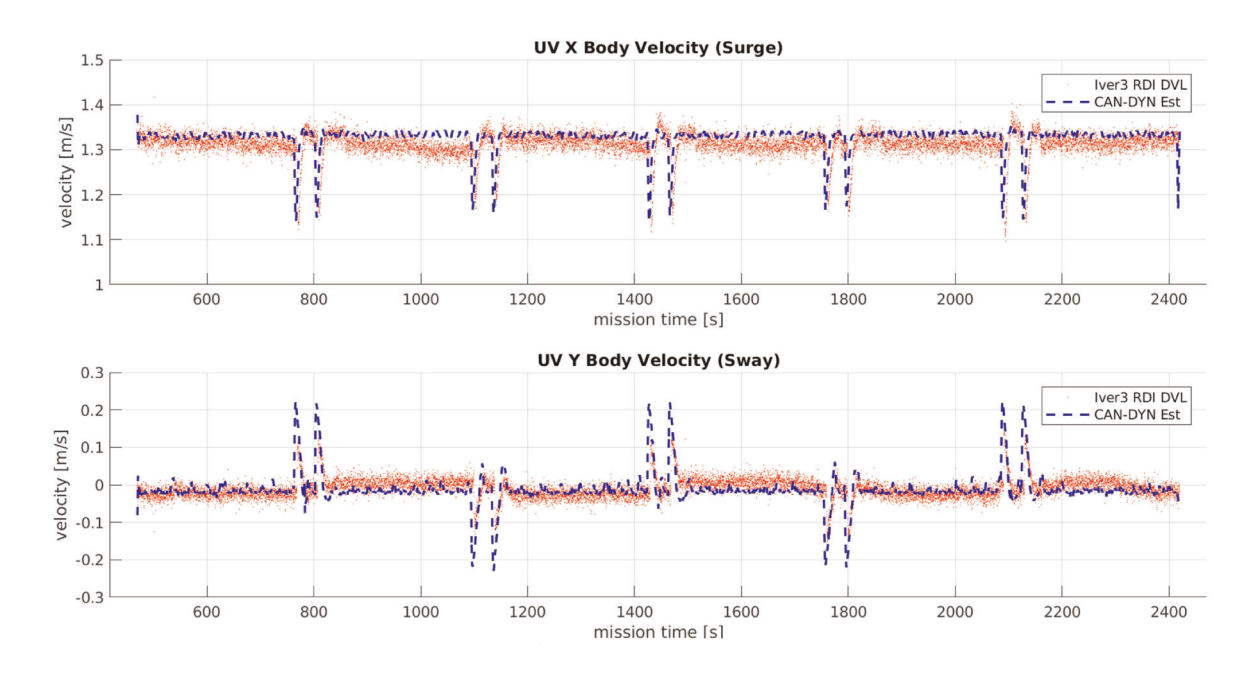


FIGURE 3 CAN-DYN without a DVL velocity estimation, Dive 55. The red dots are the Iver3 AUV 600 kHz RDI DVL measurements, and the dashed blue line is the mean of the CAN-DYN state estimator's velocity estimate without DVL observations. The spikes occur when the Iver3 is turning: the surge velocity drops because the high fin angle of the Iver3's vertical fins during turns causes increased drag; the sway velocity increases when the Iver3 experiences sideslip during turns. This figure shows the ability of CAN-DYN to estimate the Iver3's velocity without a DVL. AUV, autonomous underwater vehicle; CAN, cooperative acoustic navigation; DVL, Doppler velocity log [Color figure can be viewed at wileyonlinelibrary.com]

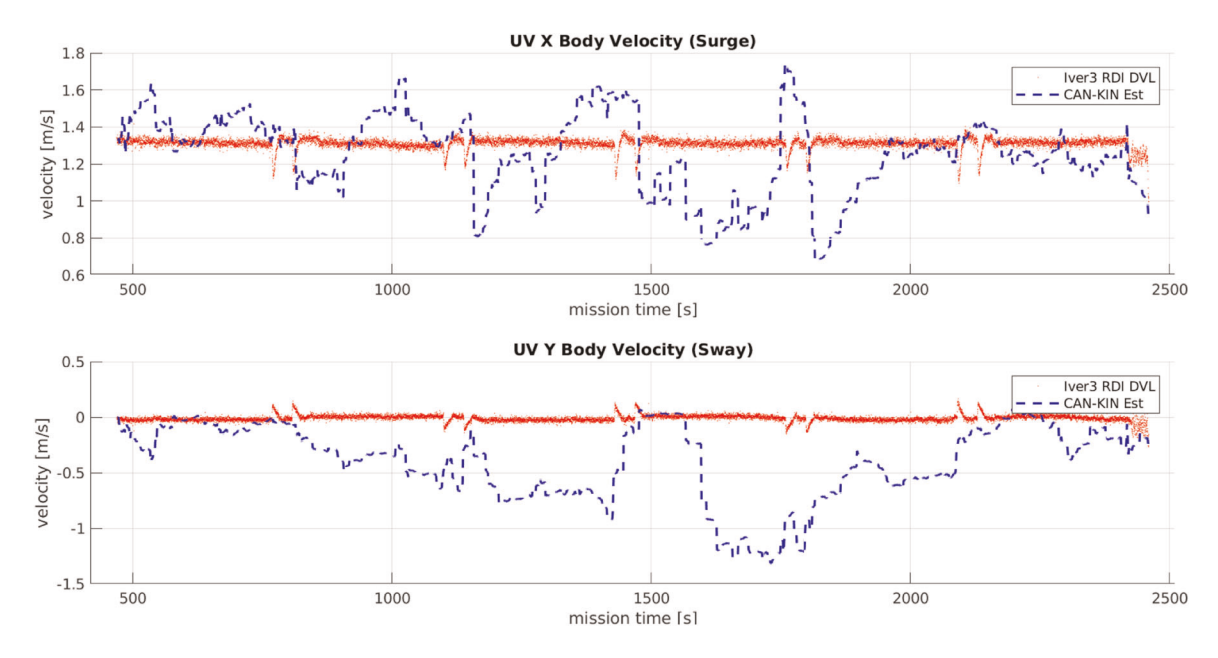


FIGURE 4 CAN-KIN without a DVL velocity estimation, Dive 55. The red dots are the Iver3 AUV 600 kHz RDI DVL measurements, and the dashed blue line is the mean of the CAN-KIN state estimator's velocity estimate. This figure shows that CAN-KIN velocity estimate performs quite poorly in both surge and sway in the absence of DVL corrections. We did not include CAN-KIN with a DVL because in that case, the CAN-KIN velocity estimate tracks the DVL measurements nearly exactly. AUV, autonomous underwater vehicle; CAN, cooperative acoustic navigation; DVL, Doppler velocity log [Color figure can be viewed at wileyonlinelibrary.com]

kinematic model to predict the UV's motion in the absence of frequent velocity observations, as seen in Figure 4. Because the position estimates from both CAN-KIN with a DVL and CAN-DYN without a DVL are stable, we do not believe the poor performance and instability of the state estimate from CAN-KIN without a DVL is caused by observability issues that arise when the relative trajectories of the surface ship and UV are not sufficiently rich and varied. However, we also note that accurate velocity estimation has little impact on the position estimate when frequent, accurate position measurements are available. A kinematic process model can provide a stable position estimate in the absence of velocity observations if frequent, high-accuracy position corrections are available. For example, Figure 2 shows the CAN-estimated ship position is stable with a purely kinematic ship process model and GPS measurements, with the navigation accuracy dependent on the sensor accuracy.

Section summary: This section reported a study comparing the performance of CAN-DYN without a DVL to CAN-KIN without a DVL, both in terms of navigation and velocity estimation. We conclude that CAN-DYN without a DVL performs well, while CAN-KIN without a DVL exhibits poor performance and quickly goes unstable in the absence of DVL observations.

5.2.2 | Experimental results: Comparison of CAN-DYN without a DVL to CAN-KIN with a DVL

This section reports a comparison of the performance of CAN-DYN without a DVL to the "gold standard" of CAN-KIN with a DVL utilizing experimental data from Dive 55.

Figure 5a shows the estimated vehicle and ship position for the "gold standard" case of CAN-KIN when the UV has access to DVL measurements for Dive 55. Figure 5b shows the position estimate from CAN-DYN without a DVL. As above, the solid black line is the waypoint trackline the vehicle attempted to follow, the dashed blue line is the CAN position estimate of the Iver3 AUV, the black dots are the CAN position estimate of the surface ship, and the red triangle is the first GPS fix after the UV surfaced. The pink ellipses are 3σ ellipses from the CAN state estimator plotted at every acoustic update.

Here again, the Iver3 AUV did not utilize the output of the various CAN state estimates as an input to the control system during the field trials, and the distance from the Iver's desired waypoint trackline is the difference between the DR track and the CAN estimate, rather than the navigation error. Indeed, the position estimates from both CAN-DYN without a DVL and CAN-KIN with a DVL diverge from the Iver3's commanded waypoint trackline. We believe this divergence occurs because the Iver3's true position diverges from the trackline, as evidenced by the position of the CAN position estimate being coincident with the first valid GPS fix obtained when the Iver3 surfaced at the end of the dive. The mission time in Figure 5 was extended until the UV surfaced, allowing the reader to observe visually that the CAN position estimate is coincident with the first valid GPS fix.

These figures show that the CAN-DYN state estimator without a DVL not only offers a stable navigation estimate, unlike CAN-KIN without a DVL, CAN-DYN without a DVL appears to perform similarly to CAN-KIN with a DVL, at least in the case of a low-cost UV, such as the Iver3 AUV operating in an area where the magnitude of

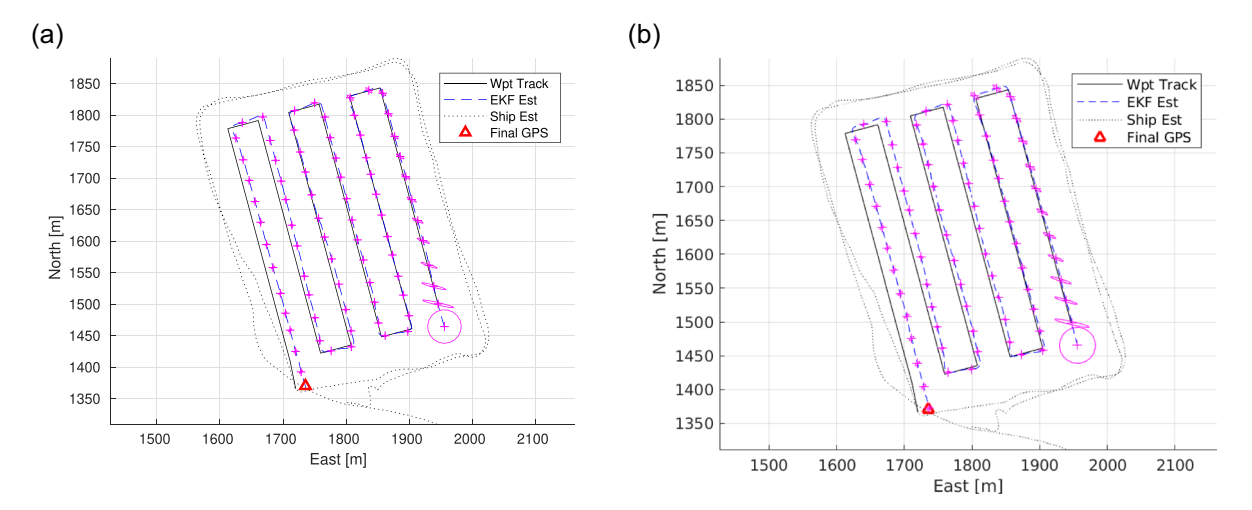


FIGURE 5 Ship and vehicle XY position estimate from experimental data from Dive 55 with the JHU Iver3 AUV in the Chesapeake Bay using (a) CAN-KIN with a DVL and (b) CAN-DYN without a DVL. The pink ellipses are 3σ ellipses from the CAN state estimator plotted at every acoustic update. As stated in Section 5.1.3, the Iver3 AUV attempted to follow the waypoint track using the manufacturer-provided navigation system (likely DR) and closed-loop control system. This figure shows that for a typical, low-cost UV like the Iver3 AUV, CAN-DYN without a DVL offers a stable position estimate that is very similar to CAN-KIN with a DVL. AUV, autonomous underwater vehicle; CAN, cooperative acoustic navigation; DR, dead reckoning; DVL, Doppler velocity log [Color figure can be viewed at wileyonlinelibrary.com]

the water-current velocity is small. This result makes sense given how well the dynamic model accurately models the submerged UV's velocity, as shown above in Figure 3.

We note that when the DVL measurements are available to *both* the CAN-KIN and CAN-DYN estimators, the performance is essentially identical—as one would expect because the DVL bottom track velocity observations exhibit very low measurement noise and high-update rate. In this case, the DVL observation innovations dominate the estimated velocity of both approaches.

Section Summary: This section reported a study comparing the performance of CAN-DYN without a DVL to the "gold standard" of CAN-KIN with a DVL. We conclude that CAN-DYN without a DVL performs on par with CAN-KIN with a DVL.

5.2.3 | Experimental results: CAN-DYN without a DVL repeatability

This section reports an investigation of the repeatability of CAN-DYN without a DVL by comparing the navigation results for two different dives that utilized identical mission plans.

The programmed mission for Dive 60 is identical to that of Dive 55 reported above: the Iver3 AUV was programmed to run a rectangular survey pattern with six $300 \, \text{m}$ legs spaced $50 \, \text{m}$ at a $2.5 \, \text{m}$ depth traveling at an advance velocity of $1.3 \, \text{m/s}$.

Figure 6 shows the mean of the CAN-estimated UV and ship XY position estimates for Iver3 Dive 60. Figure 6a shows the CAN-KIN state estimate without a DVL. Figure 6b and 6d are the same plot and shows the CAN-DYN state estimate without a DVL. Figure 6c shows the CAN-KIN state estimate with a DVL. For these plots, as above, the solid black line is the waypoint trackline the

vehicle attempted to follow, the dashed blue line is the CAN position estimate of the Iver3 AUV, the black dots are the CAN position estimate of the surface ship, and the red triangle is the first valid GPS fix after the vehicle surfaced. The pink ellipses on Figure 6b-d are 3σ ellipses plotted at every acoustic update. The 3σ ellipses are omitted from the CAN-KIN without a DVL estimate, Figure 6a, because the 3σ ellipses from the CAN-KIN state estimator without a DVL are so large the plot is unreadable.

Figure 7 shows the velocity estimate from CAN-DYN for Dive 60, and Figure 8 shows the velocity estimate from CAN-KIN without a DVL for Dive 60. As before, the red dots are the Iver3 AUV 600 kHz RDI DVL measurements, the dashed blue line is the mean of the CAN state estimator's velocity estimate, and the scale of the vertical axis is significantly larger in Figure 8 than Figure 7.

Figure 7 shows the CAN-DYN state estimator performs quite well in both surge and sway, even during turns when the UV experiences a drop in surge velocity from fin drag and an increase in sway velocity, and Figure 8 shows the constant-velocity kinematic model typically used in CAN performs poorly in the absence of a DVL.

Figures 6-8 confirm that the results reported in Sections 5.2.1 and 5.2.2 are repeatable: the CAN-KIN position estimate is poor and quickly goes unstable without velocity observations from a DVL; in contrast, the CAN-DYN state estimator does not exhibit instability and in fact, performs nearly as well as CAN-KIN with a DVL. The results from Dive 55 and Dive 60 are remarkably similar with the obvious exception of the position of the surface ship, which was piloted by a human operator and did not follow a programmed mission track. Further, these data demonstrate that a single set of model parameters can perform well across dives with the same programmed mission.

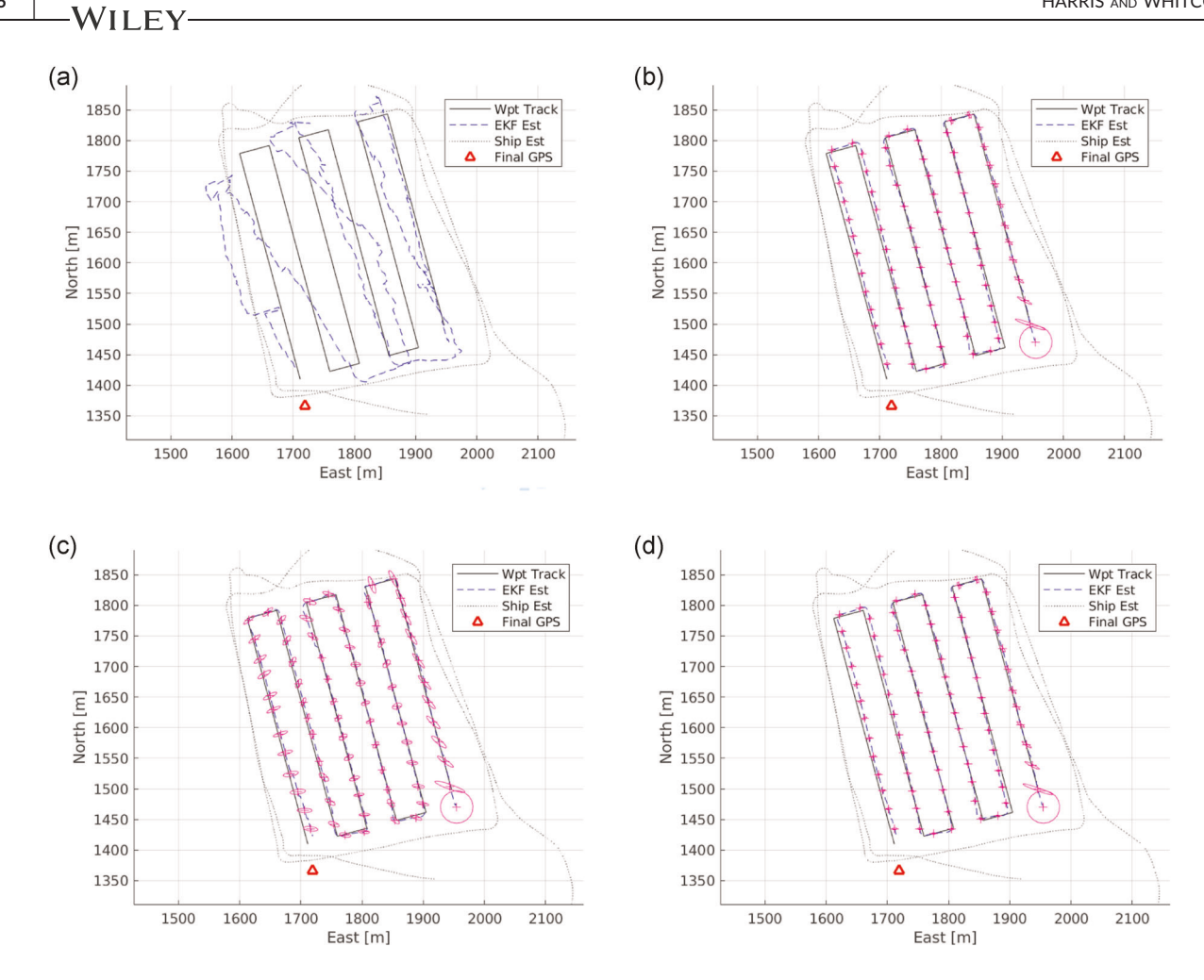


FIGURE 6 Ship and vehicle *XY* position estimate for Dive 60 using (a) CAN-KIN without a DVL, and (b) and (d) CAN-DYN, (c) CAN-KIN without a DVL on experimental data collected with the JHU Iver3 AUV in the Chesapeake Bay. The dotted black line is the CAN ship position estimate, and the dashed blue line is the CAN UV position estimate in post-processing, and the pink are the 3σ ellipses of the estimated position plotted at each acoustic update. As noted in Section 5.1.3, the position estimate from the various CAN state estimators will differ from the waypoint trackline if the UV position diverges from the waypoint trackline. This figure shows that the results from Sections 5.2.1 and 5.2.2 are repeatable. AUV, autonomous underwater vehicle; CAN, cooperative acoustic navigation; DVL, Doppler velocity log [Color figure can be viewed at wileyonlinelibrary.com]

Section Summary: This section reported an investigation of the repeatability of CAN-DYN without a DVL by comparing the navigation results for two different dives that utilized identical mission plans. XY position and velocity plots were presented, and we conclude that the CAN-DYN results are repeatable across dives with identical mission plans.

5.2.4 | Experimental results: CAN-DYN without a DVL generalizability

This section reports an investigation of the generalizability (or robustness) of CAN-DYN without a DVL by comparing the navigation results for two different dives that utilized different mission plans. In Dive 57, the vehicle ran four 300 m tracklines spaced 50 m apart while undulating from 1 to 5 m depth at a maximum vehicle pitch angle of 20 degrees. This type of undulating survey mission is very

commonly employed for conducting three-dimensional AUV surveys of water quality, in which the vehicle may be equipped with sensors for water-column properties such as conductivity, temperature, pressure, oxygen, nitrates, Ph, optical backscatter, turbidity, and fluorescence.

Figure 9 shows the mean of the CAN-estimated UV and ship XY position estimates for Dive 57. Figure 9a shows the CAN-KIN state estimate without a DVL. As in Dive 55 and Dive 60, CAN-KIN performs very poorly and exhibits instability in the absence of DVL velocity observations.

Figure 10 shows the velocity estimate from CAN-DYN without a DVL for Dive 57, and Figure 11 shows the velocity estimate from CAN-KIN without a DVL for Dive 57. The red dots are the Iver3 AUV 600 kHz RDI DVL measurements, and the dashed blue line is the mean of the CAN state estimator's velocity estimate. The vertical scale is considerably larger in Figure 11 than in Figure 10. The Iver3 AUV is equipped with a depth sensor; thus, the accuracy of the

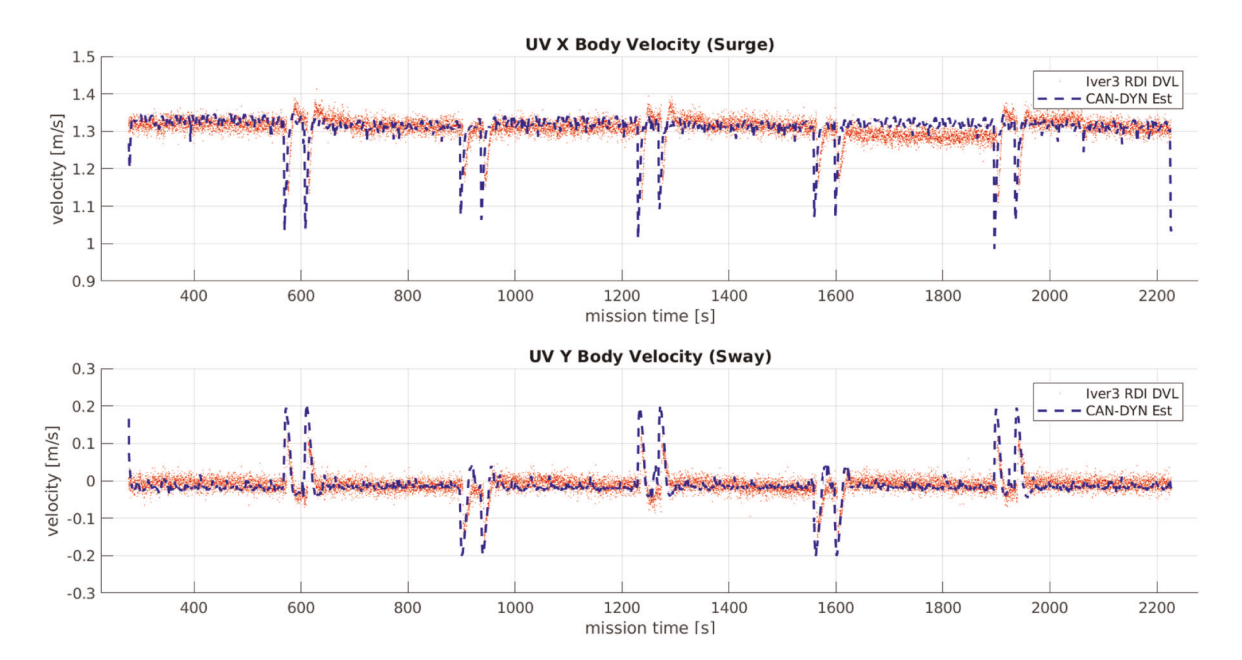


FIGURE 7 CAN-DYN without a DVL velocity estimation, Dive 60. The red dots are the Iver3 AUV 600 kHz RDI DVL measurements, and the dashed blue line is the mean of the CAN-DYN state estimator's velocity estimate. This figure demonstrates that the performance of CAN-DYN for accurate velocity estimation is repeatable across dives with the same mission. AUV, autonomous underwater vehicle; CAN, cooperative acoustic navigation; DVL, Doppler velocity log [Color figure can be viewed at wileyonlinelibrary.com]

heave-velocity estimate has little influence on the accuracy of the depth estimate. In Dive 57, the horizontal fins are actuated significantly more than in Dives 55 and 60 because the programmed trajectory has the Iver3 AUV constantly pitching at an angle of ± 20 degrees. The increased fin actuation increases the fin drag, which

results in an increased number of dips in surge velocity, all of which increases the modeling difficulty.

The results presented here demonstrate that it is feasible to use a single set of model parameters in the dynamic model of a low-cost, torpedo-shaped UV without a DVL to achieve excellent navigation

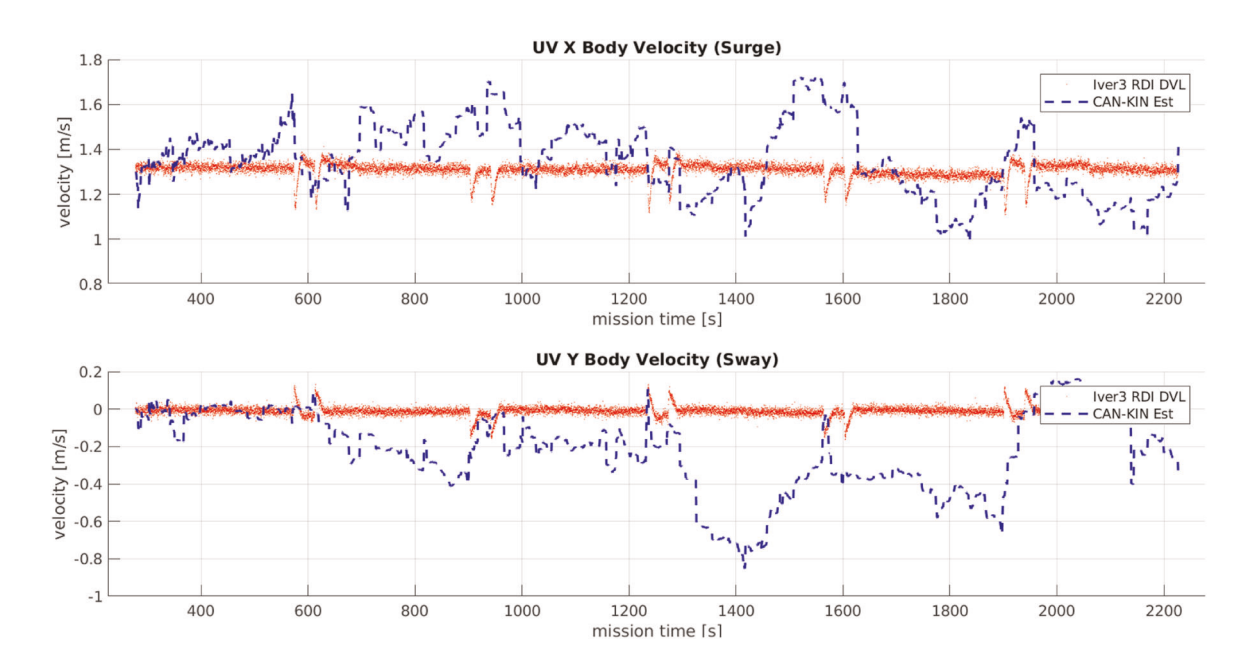


FIGURE 8 CAN-KIN without a DVL velocity estimation, Dive 60. The red dots are the Iver3 AUV 600 kHz RDI DVL measurements, and the dashed blue line is the mean of the CAN-KIN state estimator's velocity estimate. This figure shows that the poor performance of CAN-KIN without a DVL is repeatable across dives with the same mission. AUV, autonomous underwater vehicle; CAN, cooperative acoustic navigation; DVL, Doppler velocity log [Color figure can be viewed at wileyonlinelibrary.com]

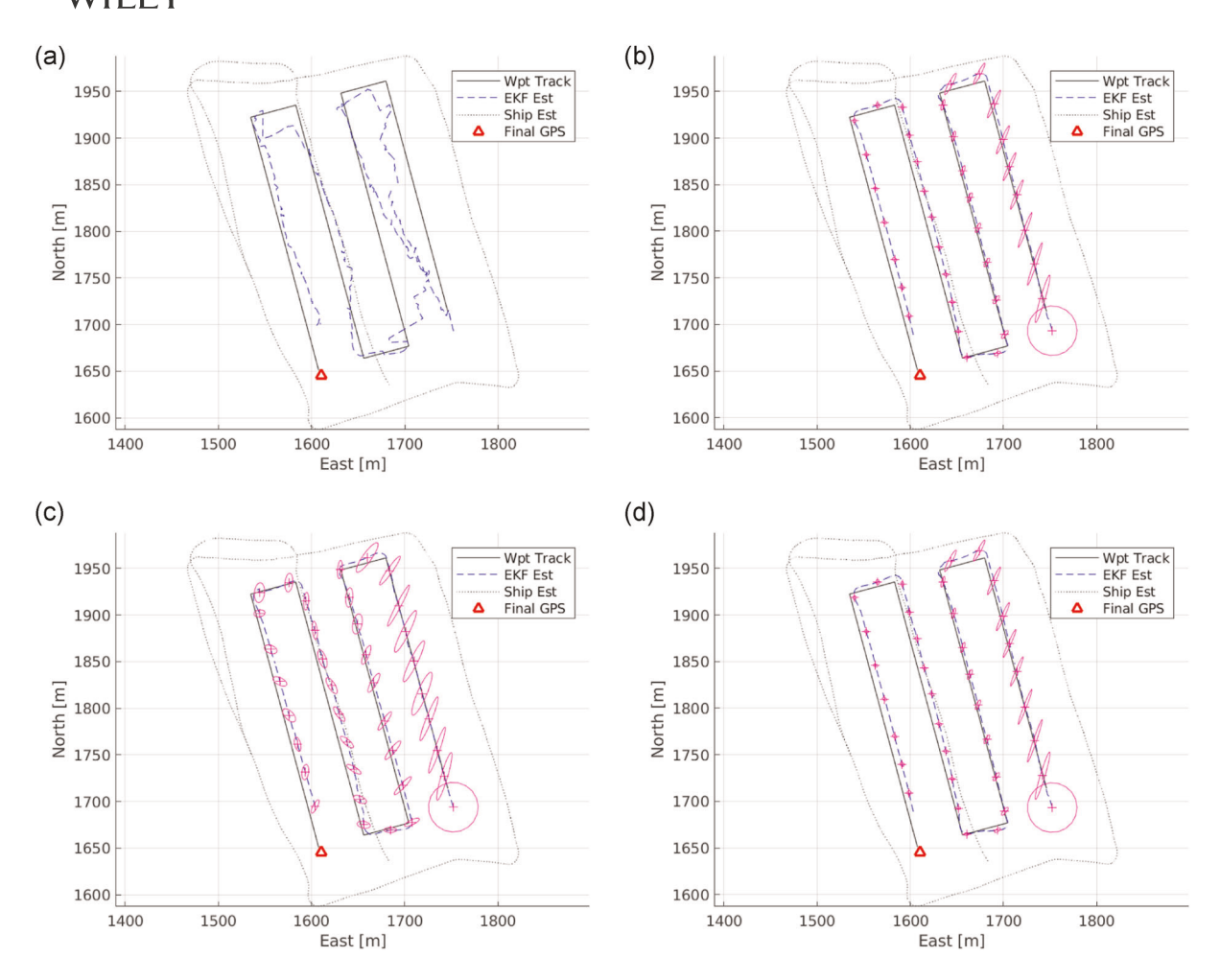


FIGURE 9 Ship and vehicle XY position estimate for Dive 57 using (a) CAN-KIN without DVL, (b) and (d) CAN-DYN (same plot), and (c) CAN-KIN with DVL on experimental data collected with the JHU Iver3 AUV in the Chesapeake Bay. The pink ellipses are 3σ ellipses from the CAN state estimator plotted at every acoustic update. In Dive 57, the Iver3 was programmed to undulate between 1 and 5 m depth at a pitch angle of 20 degrees. This figure includes only the portion of the mission before the Iver3 began its ascent to the surface near the end of the dive. This figure shows that CAN-DYN offers a stable position estimate even with an undulating depth profile, in contrast to CAN-KIN without a DVL. AUV, autonomous underwater vehicle; CAN, cooperative acoustic navigation; DVL, Doppler velocity log [Color figure can be viewed at wileyonlinelibrary.com]

results that generalize beyond the mission for which the parameters were tuned. As noted in Section 5.1.5, Dive 57 is as a cross-validation of the dynamic-model parameters, which were tuned for (constant depth) Dive 55. It is possible that tuning the parameters for a dive with some excitation in all DOF would result in a better velocity estimation, and consequently, better navigational accuracy. However, a detailed treatment of parameter estimation for dynamic UV models is beyond the scope of this paper. The purpose of this paper is to evaluate the feasibility of CAN-DYN for DVL-denied navigation of low-cost UVs. While we do not consider this to be an exhaustive result, it is strongly suggestive that the CAN algorithm parameters reported herein are not "overtuned" for one particular mission profile and perform poorly on differing mission profiles.

Section Summary: This section reported an investigation of whether CAN-DYN generalizes beyond constant-depth rectangular survey missions by comparing the navigation results for two different dives that utilized very different mission plans. XY position and

velocity plots are presented, and we conclude that the CAN-DYN without a DVL results generalize to rectangular survey missions conducted at nonconstant depth.

5.2.5 | Experimental results: CAN range-only error plots

This section reports a comparison of XY position error magnitude of CAN-DYN navigation for three dives in comparison to conventional DR navigation.

As discussed in Section 5.1.4, CAN-KIN with a DVL is the best source of ground truth for these experiments, and we call the magnitude of the difference of the XY position between CAN-KIN with a DVL and other state estimates as the "navigation error."

Figure 12 shows navigation error of CAN-DYN, as well as the navigation error of the DR track. We omit the navigation error between



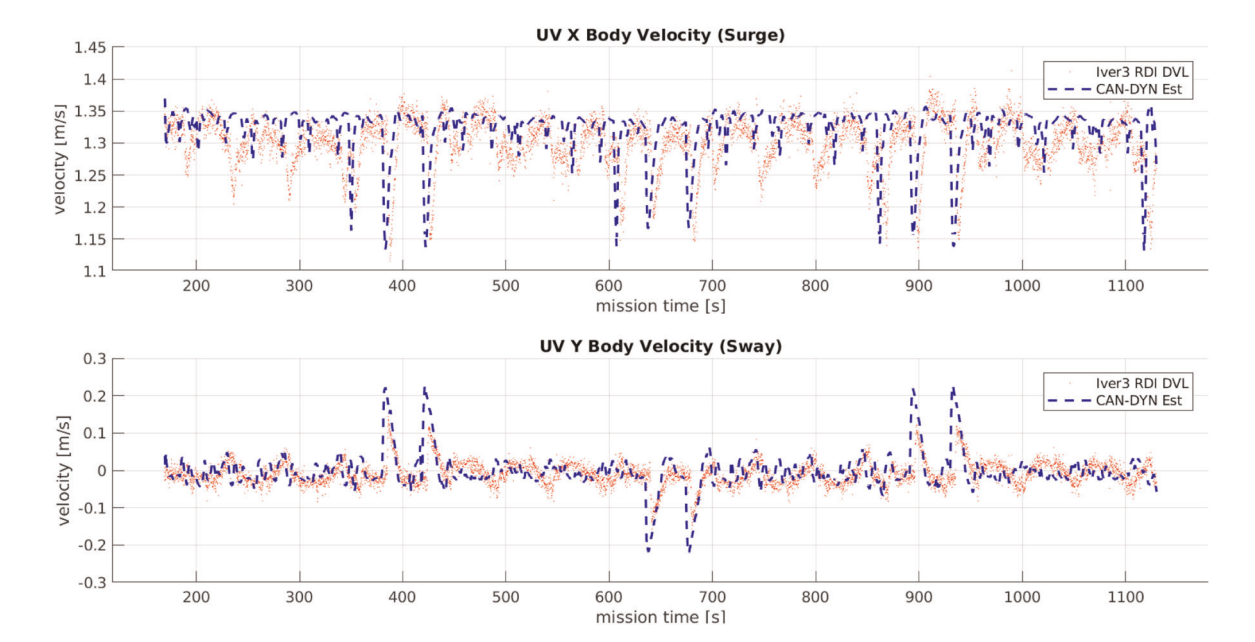


FIGURE 10 CAN-DYN without a DVL Velocity Estimation, Dive 57. In Dive 57, the Iver3 was programmed to undulate between 1 m and 5 m depth at a pitch angle of 20 degrees. This figure shows that it is feasible to use CAN-DYN for velocity estimation across multiple mission types without a DVL, even when the dynamic model parameters are not tuned for the specific mission type. AUV, autonomous underwater vehicle; CAN, cooperative acoustic navigation; DVL, Doppler velocity log [Color figure can be viewed at wileyonlinelibrary.com]

CAN-KIN without a DVL for reasons of figure scale and readability. The mission length of each dive is different: Dive 55 is approximately 2400 s; Dive 60 is approximately 2300 s; and Dive 57 is approximately 1150 s.

Figure 12 shows that the CAN-DYN position estimate stays within 8 m of the position estimate from CAN-KIN with a DVL for all three dives.

Figure 12 also illustrates the advantage of bounded-error position estimation from CAN-DYN compared with DR for low-cost UVs. The DR track is the Iver3's onboard position estimate using the manufacturer-supplied DR algorithm, which fuses the Iver3 compass data and the RDI Explorer 600 kHz DVL. Previously reported results have shown that DVL-based DR performs well when the UV is

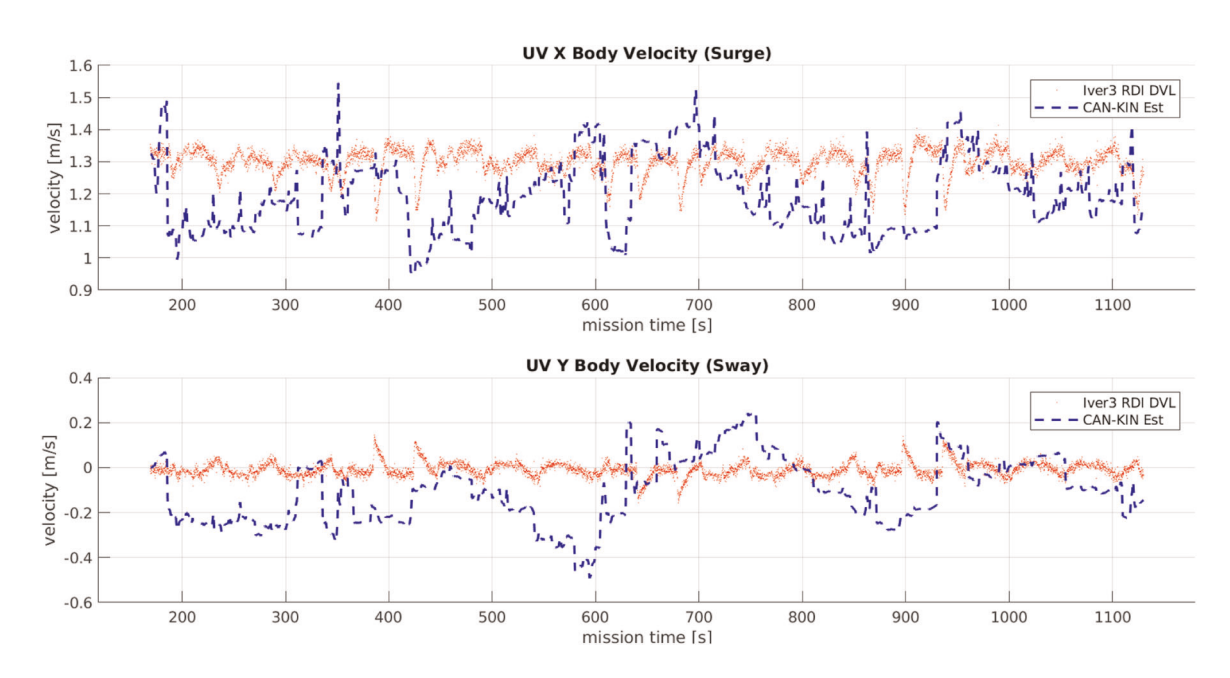


FIGURE 11 CAN-KIN without a DVL velocity estimation, Dive 57. As was the case with Dive 55 and Dive 60, CAN-KIN without a DVL provides a poor estimate of transitional velocity in surge and sway. AUV, autonomous underwater vehicle; CAN, cooperative acoustic navigation; DVL, Doppler velocity log [Color figure can be viewed at wileyonlinelibrary.com]

equipped with a high-end INS (Kinsey & Whitcomb, 2004), but the accuracy of DR is highly dependent on the accuracy of the INS; however, a high-end INS is typically far too large and far too expensive to be installed on a small, low-cost UV like the Iver3 AUV. However, as shown in Figure 12, these results may not hold for low-cost UVs equipped with a low-end compass.

The cost of an underwater acoustic modem system to enable UV CAN is less than the cost of a DVL, and the modem also provides a means for real-time acoustic telemetry to and from the UV. Before the CAN-DYN approach, low-cost UVs were often equipped a DVL instead of a CAN system if the user could not afford both sensors. There was no other choice: DR provides a stable position estimate while CAN-KIN without a DVL performs very poorly. However, Figure 12 illustrates that CAN-DYN outperforms DR for approximately the same cost and offers bounded-error position estimation.

Figure 13 shows the translation velocity error in all three DOF for the three Iver3 dives, Dive 55, Dive 60, and Dive 57. The velocity error is computed as the difference of the CAN-DYN-estimated and true velocity measured by the Iver3's RDI Explorer 600 kHz DVL. As is reported in Table 1, the RDI Explorer 600 kHz DVL measures translations velocity at 5 Hz with a standard deviation of 1.4 cm/s.

Section Summary: This section reported a comparison of XY position and velocity error of CAN-DYN without DVL for three dives in comparison to conventional DR navigation, using the CAN-KIN with DVL and the Iver3's onboard RDI Explorer 600 kHz DVL as ground truth for position and velocity, respectively. We conclude that CAN-DYN without a DVL outperforms conventional DR navigation, and CAN-DYN offers bounded-error navigational for approximately the same cost as conventional DR.

5.3 | Experimental results: CAN-DYN utilizing acoustic range and acoustic range-rate observations

This section compares CAN-DYN without a DVL utilizing acoustic range observations to CAN-DYN without a DVL utilizing acoustic range-rate observations in addition to acoustic range observations.

In previously published results, we reported that the addition of range-rate observations to acoustic range observations does not significantly improve the accuracy of the CAN-KIN state estimator in simulation, either with a DVL (Harris & Whitcomb, 2015) or without a DVL (Harris & Whitcomb, 2016). Our continued interest in acoustic range-rate observations, which are essentially observations of the relative velocity between the ship and the submerged UV, is that the range-rate is already computed by the WHOI Micromodem II and not currently utilized. In this section, we revisit the effect of adding acoustic range-rate observations to acoustic range observations on the performance of the CAN-DYN state estimator without a DVL on experimental data gathered with the Iver3 AUV in the Chesapeake Bay.

As noted above in Section 5.1.4, we use CAN-KIN with a DVL as the ground truth for these plots and all uses of the term "navigation error" are as per this definition.

Figure 14 shows the navigation error of the CAN-DYN state estimator (without a DVL) with and without the range-rate observations. The two plotted signals in Figure 14 are indistinguishable, indicating the addition of acoustic range-rate observations to acoustic range observations does not significantly improve the navigation solution from the CAN-DYN state estimator without velocity observations from a DVL in the situation of accurate model

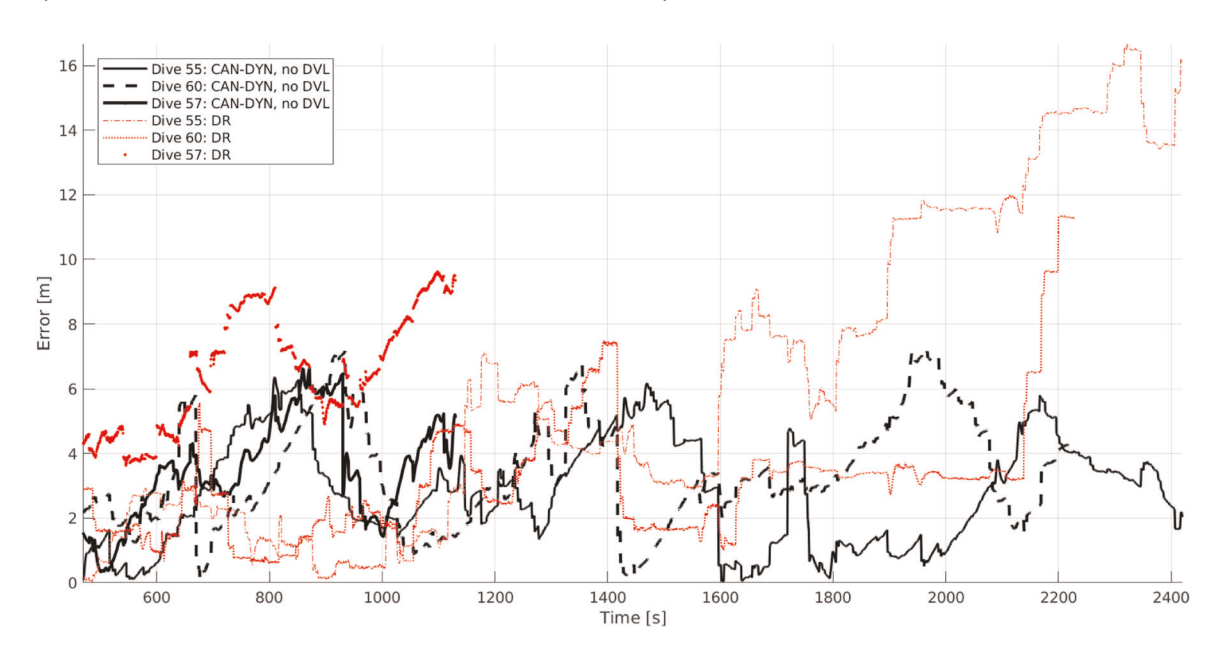


FIGURE 12 XY position error magnitude from CAN-KIN with a DVL. We do not have access to true position underwater, so we use CAN-KIN with DVL as the truth. For scale and readability reasons, the unstable state estimate from the CAN-KIN without a DVL is omitted from the figure. This figure shows that CAN-DYN without a DVL state estimate performs quite well and stays within 8 m of the CAN-KIN with a DVL state estimate for all dives. The figure also illustrates the advantage of CAN-DYN state estimation in providing bounded-error position estimates, even without a DVL, compared with dead reckoning. CAN, cooperative acoustic navigation; DVL, Doppler velocity log [Color figure can be viewed at wileyonlinelibrary.com]

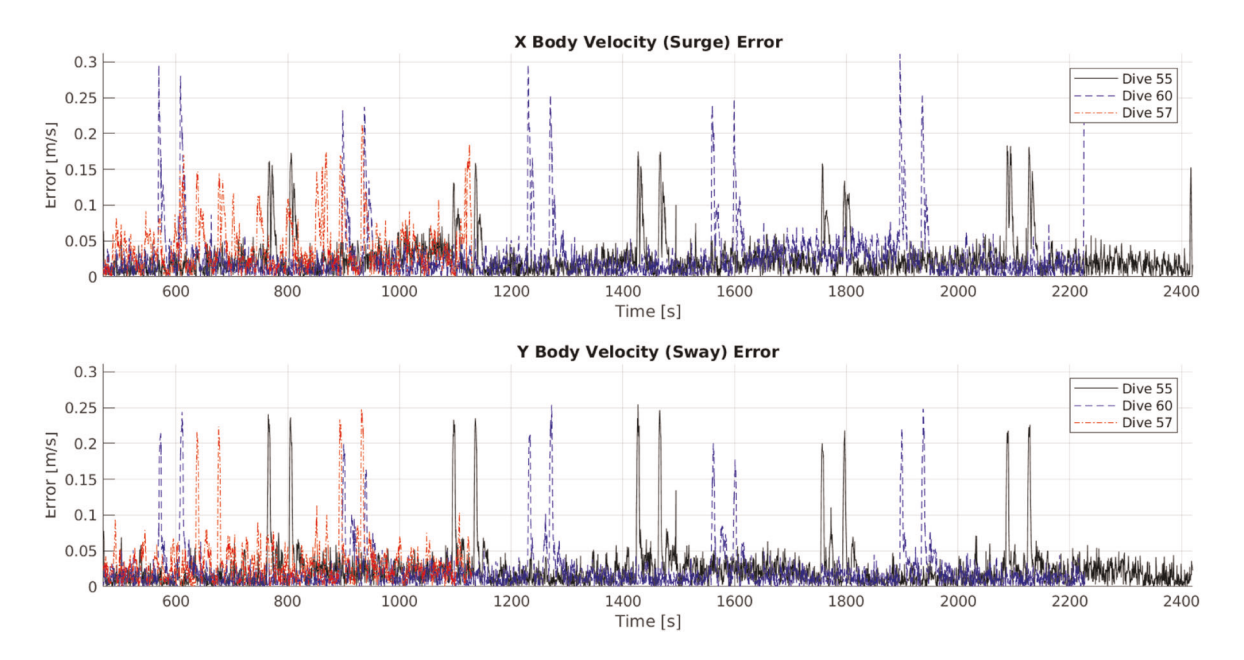


FIGURE 13 CAN-DYN velocity error from Iver3-mounted RDI 600 kHz DVL. This figure shows that the velocity estimate from CAN-DYN without a DVL for all three dives stays below approximately 30 cm/s. The velocity error is computed as the difference of the CAN-DYN-estimated and true velocity measured by the Iver3's RDI Explorer 600 kHz DVL. As is reported in Table 1, the RDI Explorer 600 kHz DVL measures transnational velocity at 5 Hz with a standard deviation of 1.4 cm/s. CAN, cooperative acoustic navigation; DVL, Doppler velocity log [Color figure can be viewed at wileyonlinelibrary.com]

coefficients, low process noise, and minimal environmental disturbances, such as water currents.

Similar results are achieved with an increase in the process noise of the CAN-DYN state estimator. Figure 15 shows the navigation error with the process noise doubled for both acoustic range and acoustic range-rate observations and acoustic range-only observations. The two signals are indistinguishable, indicating the addition of acoustic range-rate observations to acoustic range observations does not significantly improve CAN-DYN performance using high process-noise.

Additionally, we briefly investigated the performance of the CAN-DYN state estimator utilizing acoustic range and acoustic range-rate observations in the presence of modeling error of the vehicle dynamics in the form of inaccuracies in the dynamic model parameters. In our previous paper on parameter identification of low-cost, torpedo-shaped vehicles with applications to CAN (Harris et al., 2018), we showed that accurate model parameters are vital to the accuracy of the CAN-DYN state estimate without a DVL on simulated data utilizing range-only measurements. This result makes intuitive sense because the CAN state estimator relies entirely on the UV process model for velocity predictions in the absence of external velocity corrections from a DVL. Figure 16 reports the error with the mass and quadratic drag coefficients accurate to within 95% of the original values. Again, the two signals are indistinguishable, indicating the addition of acoustic range-rate observations to acoustic range observations does not significantly improve the performance of the CAN-DYN state estimator using degraded model coefficients. Figure 16 shows that the accuracy of the CAN-DYN

state estimator with range and range-rate observations is also highly dependent on the accuracy of dynamic model parameters.

We note the following two observations:

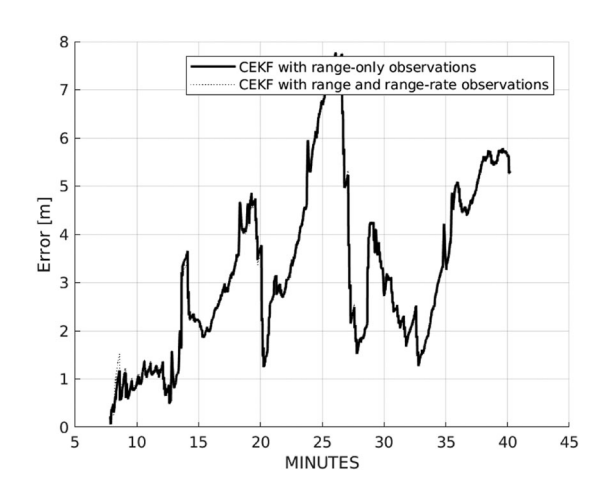


FIGURE 14 XY position error magnitude from the CAN-DYN state estimator using experimental data collected with the Iver3 AUV. The purpose of this graph is to compare the performance of CAN-DYN without a DVL using acoustic range and range-rate to that of CAN-DYN without a DVL using acoustic range-only observations. The two plotted signals are indistinguishable, indicating the addition of acoustic range-rate observations to acoustic range observations does not significantly improve the navigation solution from the CAN-DYN state estimator without velocity observations from a DVL. AUV, autonomous underwater vehicle; CAN, cooperative acoustic navigation; DVL, Doppler velocity log

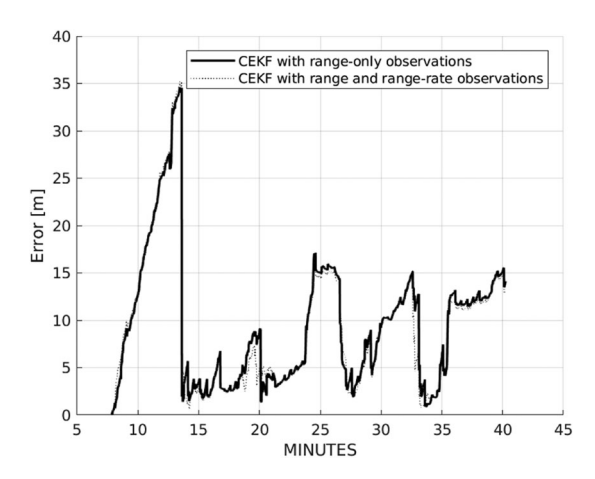


FIGURE 15 XY position error magnitude from CAN-DYN *utilizing* high process noise and no DVL using experimental data collected with the Iver3 AUV. The purpose of this graph is to compare the performance of the CAN-DYN state estimator using acoustic range and range-rate to CAN-DYN using acoustic range-only observations in the context of high process noise in the CEKF. The two signals are indistinguishable, indicating the addition of acoustic range-rate observations to acoustic range observations does not significantly improve CAN-DYN performance using high process-noise. AUV, autonomous underwater vehicle; CAN, cooperative acoustic navigation; DVL, Doppler velocity log

First, the covariance of the ship velocity must be smaller than the covariance of the UV's velocity; otherwise, the relative-velocity correction is applied to the ship's velocity instead of the submerged vehicle's velocity.

Second, the velocity covariance for a purely kinematic model will grow unbounded with time without position or velocity corrections. However, the velocity covariance of a second-order dynamic model with quadratic drag (15) will converge to a steady-state value that depends on the process noise. With a dynamic model, infrequent velocity corrections, as are provided with acoustic range-rate observations, have little net effect on the velocity or velocity covariance. If the variance of the velocity measurement is higher than the variance of the estimated velocity, the measurement will have little effect. If the variance of infrequent velocity measurements is lower than the covariance of the CAN-DYN velocity estimate, the measurement will decrease the velocity covariance at the instant the measurement is applied. However, the velocity covariance will quickly return to the steady-state value governed by the process noise associated with the second-order dynamics.

We believe the above two observations explain why the addition of acoustic range-rate observations to acoustic range does not significantly improve the state estimate from CAN-DYN without a DVL. We have no cause to believe the acoustic range rate velocity measurements gathered in these experiments suffer from a lack of observability, and therefore, we do not believe the results would be improved for different relative trajectories for the ship and UV.

Section Summary: This section reported a comparison of CAN-DYN without a DVL utilizing acoustic range observations to

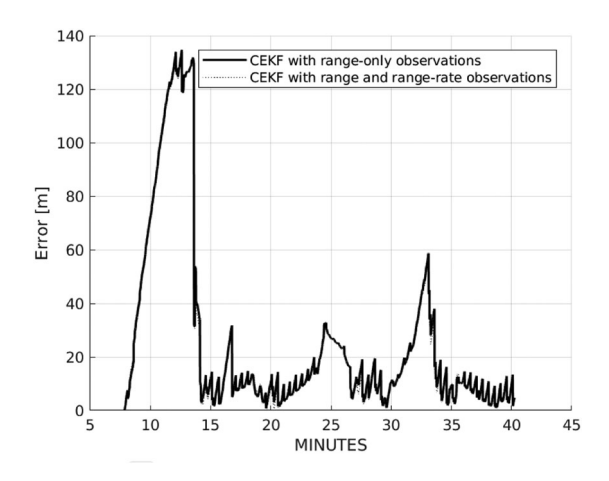


FIGURE 16 XY position error magnitude from CAN-DYN with model coefficients that have a random error with a standard deviation of 5% of the true model-parameter value using experimental data collected with the Iver3 AUV. The purpose of this graph is to compare the position estimate using acoustic range and range-rate to the CAN-DYN state estimator using acoustic range-only observations in the context of dynamic model inaccuracies. The two signals are indistinguishable, indicating the addition of acoustic range-rate observations to acoustic range observations does not significantly improve the performance of the CAN-DYN state estimator using degraded model coefficients. A second key point is how poor the error is with minor model inaccuracies. AUV, autonomous underwater vehicle; CAN, cooperative acoustic navigation

CAN-DYN without a DVL utilizing acoustic range-rate observations in addition to acoustic range observations with experimental data from Dive 55. We conclude that the addition of acoustic range-rate observations to acoustic range does not significantly improve the CAN-DYN without a DVL state estimate.

6 | CONCLUSION

This paper reports theory and experimental results for use of a second-order nonlinear dynamic model of UVs in CAN. We utilize the CEKF formulation of CAN with one UV client (equipped with acoustic modem, attitude, and depth sensors) with one surface vehicle server (equipped with GPS and an acoustic modem). We develop a second-order nonlinear dynamical model of submerged UV motion, including development of the nonlinear actuation function to map the commanded fin angle and propeller speed to an overall force-moment vector on the UV, for use in CAN-DYN.

The main contributions and conclusions from the paper are detailed in Section 5 and are the following:

- Section 5.2 reports a comparative performance analysis of CAN-DYN and CAN-KIN using acoustic range-only observations from three dives.
 - a. Section 5.2.1 reports a comparison of the performance of CAN-DYN to CAN-KIN, both without a DVL. XY position and

velocity plots are presented. We conclude that CAN-DYN without a DVL performs well, while CAN-KIN without a DVL exhibits poor performance and quickly goes unstable in the absence of DVL observations.

- b. Section 5.2.2 reports a comparison of the performance of CAN-DYN without a DVL to the "gold standard" of CAN-KIN with a DVL. We conclude that CAN-DYN without a DVL performs on par with CAN-KIN with a DVL.
- c. Section 5.2.3 reports an investigation of the repeatability of CAN-DYN without a DVL by comparing the navigation results for two different dives that utilized identical mission plans. XY position and velocity plots are presented, and we conclude that the CAN-DYN results are repeatable across dives with identical mission plans.
- d. Section 5.2.4 reports an investigation of the generalizability of CAN-DYN by comparing the navigation results for two different dives that utilized very different mission plans. XY position and velocity plots are presented, and we conclude that the CAN-DYN results generalize to rectangular survey missions conducted at nonconstant (undulating) depth.
- e. Section 5.2.5 reports a comparison of XY position error magnitude of CAN-DYN without DVL navigation for three dives in comparison to conventional DR navigation, using the CAN-KIN with DVL as ground truth. Also reported is a comparison of the XY velocity error for the CAN-DYN state estimator without a DVL, computed as the difference between the CAN-DYN velocity estimate and the Iver3's RDI Explorer 600 kHz DVL. We conclude that CAN-DYN without a DVL outperforms conventional DR navigation, and CAN-DYN offers bounded-error navigational for approximately the same cost as conventional DR.
- 2. Section 5.3 reports results from Dive 55 comparing CAN-DYN without a DVL utilizing acoustic range observations to CAN-DYN without a DVL utilizing acoustic range-rate observations in addition to acoustic range observations. We conclude that the addition of acoustic range-rate observations to acoustic range does not significantly improve the CAN-DYN without a DVL state estimate.

6.1 | Analysis

Unlike other positioning systems (e.g., 1 Hz GPS position fixes for surface and aerial vehicles), position corrections provided by OWTT CAN for fully submerged vehicles are infrequent and nonunique. In the interval of time between acoustic position corrections, the CAN state estimator uses the estimated velocity to propagate the estimated position mean and covariance, in accordance with the process model. Thus, accurate velocity estimation is crucial to accurate position estimation. We conclude that the poor performance and instability of the position estimate from CAN-KIN EKF without a DVL is caused by the inability of a kinematic model to predict the UV's motion in the absence of frequent external position and velocity observation corrections. Because the position estimates from CAN-KIN with a DVL and CAN-DYN without a DVL are both stable, we have no reason to believe the poor performance

and instability of the state estimate from CAN-KIN without a DVL is caused by observability issues arising from insufficiently rich and varied relative trajectories of the surface ship and UV.

6.2 | Limitations of CAN-DYN

Although CAN-DYN appears to outperform CAN-KIN without a DVL, we take care to note several limitations and considerations regarding the CAN-DYN approach. A primary consideration is that the accuracy of the navigation solution of CAN-DYN without a DVL depends nearly entirely on the accuracy of the parameters for the dynamic model (Harris et al., 2018). Anecdotally, as evidenced by our previously reported simulation study on range-rate using CAN-KIN without a DVL (Harris & Whitcomb, 2016), CAN-KIN may perform significantly better for certain ship-vehicle geometries with a highend AHRS, at least in simulation. However, these preliminary simulation results have not been validated with experimental data. Additionally, low-cost UVs like the JHU Iver3 AUV are typically equipped with a magnetic compass—it is rare to have access to a high-end AHRS, such as FOG, on a low-cost UV.

6.3 | Future work

Although the focus of this paper is a comparison of kinematic and dynamic process models, and the effect of range-rate, on CAN, the reported approaches can be extended to include the simultaneous estimation of UV state and ambient water-current velocity, as has been studied extensively, for example, Claus et al. (2017), Crasta et al. (2013, 2014), Gadre and Stilwell (2005a, 2005b), Gallimore et al. (2019). Hegrenas et al. (2008), Webster et al. (2015).

ACKNOWLEDGMENTS

We gratefully acknowledge the support of the National Science Foundation under Awards 1319667 and 1909182, and the Office of Naval Research under a National Defense Science and Engineering Graduate Fellowship. Harris was with the Department of Mechanical Engineering, Johns Hopkins University, Baltimore, Maryland, USA, and is presently with the Charles Stark Draper Laboratory, Cambridge, MA, USA. We gratefully acknowledge using and extending, with permission, a centralized extended Kalman filter (CEKF) implementation originally developed by our colleague Dr. Ryan Eustice at the University of Michigan and subsequently extended by Dr. Sarah Webster who is presently with the University of Washington Applied Physics Laboratory. We are grateful to Mr. Rick and Ms. Valerie Smith, owners of Smiths Marina, Crownsville, MD, for their gracious support of the JHU Iver3 AUV field trials reported herein, and to Captain John Sharp of the F/V Miss Molly of Stevensville, MD.

ORCID

Zachary J. Harris https://orcid.org/0000-0002-5498-301X **Louis L. Whitcomb** https://orcid.org/0000-0003-2398-1000

WILEY-

REFERENCES

- Alleyne, J. (2000). Position estimation from range only measurements (Master's thesis). Naval Postgraduate School, Monterey, CA.
- Arrichiello, F., Antonelli, G., Aguiar, A., & Pascoal, A. (2013). An observability metric for underwater vehicle localization using range measurements. Sensors, 13(12), 16191–16215.
- Baccou, P., & Jouvencel, B. (2002). Homing and navigation using one transponder for AUV, post-processing comparisons results with long base-line navigation. In *Proceedings of the IEEE International* Conference on Robotics and Automation (Vol. 4, pp. 4004–4009). Institute of Electrical and Electronics Engineers (IEEE).
- Baccou, P., & Jouvencel, B. (2003). Simulation results, post-processing experimentations and comparisons results for navigation, homing and multiple vehicles operations with a new positioning method using on transponder. In *Proceedings of the IEEE/RSJ International Conference on Intelligent Robots and Systems* (Vol. 1, pp. 811–817). Institute of Electrical and Electronics Engineers (IEEE).
- Bahr, A. (2009). Cooperative localization for autonomous underwater vehicles (PhD thesis). Joint Program in Applied Ocean Science and Engineering, Massachusetts Institute of Technology and the Woods Hole Oceanographic Institution. Cambridge MA and Woods Hole. MA.
- Bahr, A., & Leonard, J. (2006). Cooperative localization for autonomous underwater vehicles. In *Proceedings of the 10th International Symposium on Experimental Robotics (ISER)* (pp. 387–395). Springer-Verlag Berlin Heidelberg. https://doi.org/10.1007/978-3-540-77457-0, https://www.springer.com/gp/book/9783540774563
- Bahr, A., Leonard, J. J., & Fallon, M. F. (2009). Cooperative localization for autonomous underwater vehicles. *International Journal of Robotics Research*, 28(6), 714–728.
- Bailey, T., Bryson, M., Mu, H., Vial, J., McCalman, L., & Durrant-Whyte, H. (2011). Decentralised cooperative localisation for heterogeneous teams of mobile robots. In *Proceedings of IEEE International Conference on Robotics and Automation* (pp. 2859–2865). Institute of Electrical and Electronics Engineers (IEEE).
- Bar-Shalom, Y., Rong Li,X., & Kirubarajan, T. (2001). Estimation with applications to tracking and navigation, New York: John Wiley & Sons. Inc.
- Batista, P. (2015). Long baseline navigation with clock offset estimation and discrete-time measurements. *Control Engineering Practice*, *35*, 43–53.
- Batista, P., Silvestre, C., & Oliveira, P. (2010). Single beacon navigation: Observability analysis and filter design. In *Proceedings of the 2010 American Control Conference* (pp. 6191–6196). Institute of Electrical and Electronics Engineers (IEEE).
- Batista, P., Silvestre, C., & Oliveira, P. (2011). Single range aided navigation and source localization: Observability and filter design. *Systems & Control Letters*, 60(8), 665–673.
- Batista, P., Silvestre, C., & Oliveira, P. (2014). Sensor-based long baseline navigation: Observability analysis and filter design. *Asian Journal of Control*, 16(4), 974–994.
- Bellingham, J., Deffenbaugh, M., Leonard, J., & Catipovic, J. (1994). Arctic under-ice survey operations. *Unmanned Systems*, 12, 24–29.
- Bourgeois, B. S. (2007). Using range and range rate for relative navigation (technical report). Stennis Space Center, MS: Naval Research Laboratory, Mapping, Charting, Geodesy Branch, Marine Geosciences Division.
- Catipovic, J. A., & Freitag, L. E. (1990). High data rate acoustic telemetry for moving ROVs in a fading multipath shallow water environment. In Proceedings of the Symposium on Autonomous Underwater Vehicle Technology (pp. 296–303). Institute of Electrical and Electronics Engineers (IEEE).
- Chatfield, A. (1997). Fundamentals of high accuracy inertial navigation (Vol. 174). American Institute of Aeronautics & Astronautics (AIAA).

- Claus, B., Kepper, J. H., Suman, S., & Kinsey, J. C. (2017). Closed-loop oneway-travel-time navigation using low-grade odometry for autonomous underwater vehicles. *Journal of Field Robotics*, 35(4), 421–434.
- Crasta, N., Bayat, M., Aguiar, A. P., & Pascoal, A. M. (2013). Observability analysis of 2D single beacon navigation in the presence of constant currents for two classes of maneuvers. *IFAC Proceedings Volumes*, 46(33), 227–232.
- Crasta, N., Bayat, M., Aguiar, A. P., & Pascoal, A. M. (2014). Observability analysis of 3D AUV trimming trajectories in the presence of ocean currents using single beacon navigation. *IFAC Proceedings Volumes*, 47(3), 4222–4227.
- Crasta, N., Moreno-Salinas, D., Pascoal, A., & Aranda, J. (2018). Multiple autonomous surface vehicle motion planning for cooperative rangebased underwater target localization. *Annual Reviews in Control*, 46, 326–342.
- De Palma, D., Arrichiello, F., Parlangeli, G., & Indiveri, G. (2017).

 Underwater localization using single beacon measurements:

 Observability analysis for a double integrator system. *Ocean Engineering*, 142, 650–665.
- Eustice, R. M., Camilli, R., & Singh, H. (2005). Towards bathymetryoptimized Doppler re-navigation for AUVs. In *Proceedings of the IEEE/MTS OCEANS Conference and Exhibition* (pp. 1430–1436). Institute of Electrical and Electronics Engineers (IEEE).
- Eustice, R. M., Singh, H., & Leonard, J. J. (2006). Exactly sparse delayedstate filters for view-based SLAM. *IEEE Transactions on Robotics*, 22(6), 1100–1114.
- Eustice, R. M., Singh, H., Leonard, J. J., & Walter, M. R. (2006). Visually mapping the RMS Titanic: Conservative covariance estimates for SLAM information filters. *International Journal of Robotics Research*, 25(12), 1223–1242.
- Eustice, R. M., Singh, H., & Whitcomb, L. L. (2011). Synchronous-clock oneway-travel-time acoustic navigation for underwater vehicles. *Journal* of Field Robotics, Special Issue on State of the Art in Maritime Autonomous Surface and Underwater Vehicles, 28(1), 121–136.
- Eustice, R. M., Whitcomb, L. L., Singh, H., & Grund, M. (2006). Recent advances in synchronous-clock one-way-travel-time acoustic navigation. In *Proceedings of the IEEE/MTS OCEANS Conference and Exhibition* (pp. 1–6). Institute of Electrical and Electronics Engineers (IEEE).
- Fallon, M. F., Papadopoulos, G., Leonard, J. J., & Patrikalakis, N. M. (2010). Cooperative AUV navigation using a single maneuvering surface craft. International Journal of Robotics Research, 29(12), 1461–1474.
- Fleischer, S. (2000). Bounded-error vision-based navigation of autonomous underwater vehicles (Ph.D. thesis). Stanford University, Stanford, CA.
- Fofonoff, N., & Millard Jr., R. (1983). Algorithms for the computation of fundamental properties of seawater (UNESCO Technical Papers in Marine Sciences). Paris: UNESCO.
- Fossen, T. I. (1994). Guidance and control of ocean vehicles, New Jersey: John Wiley and Sons.
- Gadre, A. (2007). Observability analysis in navigation systems with an underwater vehicle application (Ph.D. thesis). Virginia Polytechnic Institute and State University, Blacksburg, VA.
- Gadre, A., & Stilwell, D. (2004). Toward underwater navigation based on range measurements from a single location. In *Proceedings of the IEEE International Conference on Robotics and Automation* (Vol. 5, pp. 4472–4477). Institute of Electrical and Electronics Engineers (IEEE).
- Gadre, A., & Stilwell, D. (2005a). A complete solution to underwater navigation in the presence of unknown currents based on range measurements from a single location. In *Proceedings of the IEEE/RSJ International Conference on Intelligent Robots and Systems* (pp. 1420–1425). Institute of Electrical and Electronics Engineers (IEEE).
- Gadre, A., & Stilwell, D. (2005b). Underwater navigation in the presence of unknown currents based on range measurements from a single location. Proc. Am. Control Conf. Vol. 1, 656–661. Institute of Electrical and Electronics Engineers (IEEE).

- Gaiffe, T. (2002). U-Phins: A FOG-based inertial navigation system developed specifically for AUV navigation and control. In *International Conference on Underwater Intervention*. Institute of Electrical and Electronics Engineers (IEEE).
- Gallimore, E., Anderson, M., Freitag, L., & Terrill, E. (2019). Synthetic baseline navigation using phase-coherent acoustic communication signals. The Journal of the Acoustical Society of America, 146(6), 4831–4841.
- Gallimore, E., Partan, J., Vaughn, I., Singh, S., Shusta, J., & Freitag, L. (2010). The WHOI micromodem-2: A scalable system for acoustic communications and networking. In OCEANS 2010 MTS/IEEE SEATTLE (pp. 1–7). Institute of Electrical and Electronics Engineers (IEEE).
- Garcia, R., Batlle, J., Cufi, X., & Amat, J. (2001). Positioning an underwater vehicle through image mosaicking. In *Proceedings of the IEEE International Conference on Robotics and Automation* (Vol. 3, pp. 2779–2784). Institute of Electrical and Electronics Engineers (IEEE).
- Green, M., & Scussel, K. (2007). Underwater data communication and instrument release management system. US Patent 7,187,623.
- Harris, Z. J., Paine, T. M., & Whitcomb, L. L. (2018). Preliminary evaluation of null-space dynamic process model identification with application to cooperative navigation of underwater vehicles. In 2018 IEEE/RSJ International Conference on Intelligent Robots and Systems (IROS) (pp. 3453–3459). Institute of Electrical and Electronics Engineers (IEEE).
- Harris, Z. J., & Whitcomb, L. L. (2015). Preliminary feasibility study of cooperative navigation of underwater vehicles with range and range-rate observations. In *Proceedings of the IEEE/MTS OCEANS* Conference. Institute of Electrical and Electronics Engineers (IEEE).
- Harris, Z. J., & Whitcomb, L. L. (2016). Preliminary study of cooperative navigation of underwater vehicles without a DVL utilizing range and range-rate observations. In *Proceedings of IEEE International* Conference on Robotics and Automation. Institute of Electrical and Electronics Engineers (IEEE).
- Harris, Z. J., & Whitcomb, L. L. (2018a). Preliminary evaluation of cooperative navigation of underwater vehicles without a DVL utilizing a dynamic process model. In *Proceedings of IEEE International Conference on Robotics and Automation*. Brisbane. Institute of Electrical and Electronics Engineers (IEEE).
- Harris, Z. J., & Whitcomb, L. L. (2018b). Preliminary simulation study of combined control and cooperative navigation for underwater vehicles. In *Proceedings of the IEEE/MTS OCEANS Conference*. Institute of Electrical and Electronics Engineers (IEEE).
- Hartsfield, J. C. (2005). Single transponder range only navigation geometry (STRONG) applied to REMUS autonomous under water vehicles (Master's thesis). Joint Program in Applied Ocean Science and Engineering, Massachusetts Institute of Technology and the Woods Hole Oceanographic Institution. Cambridge MA and Woods Hole. MA.
- Hegrenas, O., Berglund, E., & Hallingstad, O. (2008). Model-aided inertial navigation for underwater vehicles. In 2008 IEEE International Conference on Robotics and Automation (pp. 1069–1076).
- Hermann, R., & Krener, A. (1977). Nonlinear controllability and observability. IEEE Transactions on Automatic Control, 22(5), 728–740.
- Hung, N. T., Crasta, N., Moreno-Salinas, D., Pascoal, A. M., & Johansen, T. A. (2020). Range-based target localization and pursuit with autonomous vehicles: An approach using posterior CRLB and model predictive control. *Robotics and Autonomous Systems*, 132, 103608.
- Hunt, M., Marquet, W., Moller, D., Peal, K., Smith, W., & Spindel, R. (1974).
 An acoustic navigation system (Technical Report WHOI-74-6).
 Woods Hole, MA: Woods Hole Oceanographic Institution.
- Jakuba, M. V., Roman, C. N., Singh, H., Murphy, C., Kunz, C., Willis, C., Sato, T., & Sohn, R. A. (2008). Long-baseline acoustic navigation for under-ice autonomous underwater vehicle operations. *Journal of Field Robotics*, 25(11–12), 861-879.

- Jouffroy, J., & Reger, J. (2006). An algebraic perspective to single-transponder underwater navigation. In *Proceedings IEEE 2006 CCA/CACSD/ISIC* (pp. 1789–1794). Institute of Electrical and Electronics Engineers (IEEE).
- Kepper, J. H., IV, Claus, B. C., & Kinsey, J. C. (2019). A navigation solution using a MEMS IMU, model-based dead-reckoning, and one-way-traveltime acoustic range measurements for autonomous underwater vehicles. IEEE Journal of Oceanic Engineering, 44(3), 664–682.
- Kilfoyls, D. B., & Baggeroer, A. B. (2000). The state of the art in underwater acoustic telemetry. *IEEE Journal of Oceanic Engineering*, 25(1), 4–27. Institute of Electrical and Electronics Engineers (IEEE).
- Kinsey, J. C., Eustice, R. M., & Whitcomb, L. L. (2006). A survey of underwater vehicle navigation: Recent advances and new challenges. In *IFAC Conference of Manoeuvring and Control of Marine Craft*. International Federation of Automatic Control.
- Kinsey, J. C., & Whitcomb, L. L. (2004). Preliminary field experience with the DVLNAV integrated navigation system for oceanographic submersibles. Control Engineering Practice, 12(12), 1541–1549.
- L3 OceanServer. (2015). OceanServer. (2015). Digital Compass Users Guide, OS5000 Series (Rev. 5.0 ed.). OceanServer.
- L3 OceanServer. (2016). AUV Operating Guide (Rev. 5.0 ed.). OceanServer. LaPointe, C. E. (2006). Virtual long baseline (VLBL) autonomous underwater vehicle navigation using a single transponder (Master's thesis). Joint Program in Applied Ocean Science and Engineering, Massachusetts Institute of Technology and the Woods Hole Oceanographic Institution. Cambridge MA and Woods Hole, MA.
- Larsen, M. (2000a). High performance Doppler-inertial navigation-experimental results. In *Proceedings of the IEEE/MTS OCEANS Conference and Exhibition* (Vol. 2, pp. 1449–1456). Institute of Electrical and Electronics Engineers (IEEE).
- Larsen, M. (2000b). Synthetic long baseline navigation of underwater vehicles. In *Proceedings of the IEEE/MTS OCEANS Conference and Exhibition* (Vol. 3, pp. 2043–2050). Institute of Electrical and Electronics Engineers (IEEE).
- Larsen, M. (2000c). Synthetic long baseline navigation of underwater vehicles. In OCEANS 2000 MTS/IEEE Conference and Exhibition (Vol. 3, pp. 2043–2050). Institute of Electrical and Electronics Engineers (IEEE).
- Larsen, M. (2002). High performance autonomous underwater navigation: Experimental results. *Hydro International*, *6*(1), 6–9.
- Larsen, M. (2006). Methods and systems for navigating under water. US Patent 7,139,647.
- Lee, P.-M., Jun, B.-H., & Lim, Y.-K. (2008). Review on underwater navigation system based on range measurements from one reference. In OCEANS 2008 MTS/IEEE Kobe Techno-Ocean (pp. 1-5). Institute of Electrical and Electronics Engineers (IEEE).
- Martin, S. C. (2008). Advances in six-degree-of-freedom dynamics and control of underwater vehicle (Ph.D. thesis). The Johns Hopkins University, Baltimore, MD.
- McPhail, S., & Pebody, M. (2009). Range-only positioning of a deep-diving autonomous underwater vehicle from a surface ship. *IEEE Journal of Oceanic Engineering*, 34(4), 669–677.
- Milne, P. H. (1983). *Underwater acoustic positioning systems*, Houston, TX: Gulf Publishing.
- Moreno-Salinas, D., Crasta, N., Pascoal, A. M., & Aranda, J. (2019). Range-based navigation algorithms for marine applications. In C. Gao, G. Zhao, & N. Konopka (Eds.), Cooperative localization and navigation: Theory, research and practice (pp. 335–387). CRC Press.
- Moutarlier, P., & Chatila, R. (1989). An experimental system for incremental environment modeling by an autonomous mobile robot. In *Proceedings of the International Symposium on Experimental Robotics* (pp. 327–346). Springer-Verlag Berlin Heidelberg.
- Paine, T. M. (2018). Robust model identification methods for nonlinear second-order plant models for underwater vehicles (Master's thesis). Baltimore, MD: Johns Hopkins University.

- -WILEY-
- Parlangeli, G., & Indiveri, G. (2014). Single range observability for cooperative underactuated underwater vehicles. *IFAC Proceedings Volumes*, 47(3), 5127–5138.
- Partan, J., Kurose, J., & Levine, B. N. (2007). A survey of practical issues in underwater networks. ACM SIGMOBILE Mobile Computing and Communications Review, 11(4), 23–33.
- Paull, L., Seto, M., & Leonard, J. (2014). Decentralized cooperative trajectory estimation for autonomous underwater vehicles. In 2014 IEEE/RSJ International Conference on Intelligent Robots and Systems (IROS 2014) (pp. 184–191). Institute of Electrical and Electronics Engineers (IEEE).
- Quenzer, J. D., & Morgansen, K. A. (2014). Observability based control in range-only underwater vehicle localization. In 2014 American Control Conference (pp. 4702–4707). Institute of Electrical and Electronics Engineers (IEEE).
- Ristic, B., Arulampalam, S., & McCarthy, J. (2002). Target motion analysis using range-only measurements: algorithms, performance and application to ISAR data. *Signal Processing*, 82(2), 273–296.
- Roman, C. N. (2005). Self consistent Bathymetric mapping from robotic vehicles in the deep ocean (Ph.D. thesis). Joint Program in Applied Ocean Science and Engineering, Massachusetts Institute of Technology and the Woods Hole Oceanographic Institution. Cambridge MA and Woods Hole, MA.
- Ross, A., & Jouffroy, J. (2005). Remarks on the observability of single beacon underwater navigation. In *Proceedings of the International Symposium on Unmanned Untethered Submersible Technology*. Institute of Electrical and Electronics Engineers (IEEE).
- Rypkema, N. R., Fischell, E. M., & Schmidt, H. (2017). One-way travel-time inverted ultra-short baseline localization for low-cost autonomous underwater vehicles. In 2017 IEEE International Conference on Robotics and Automation (ICRA) (pp. 4920–4926). Institute of Electrical and Electronics Engineers (IEEE).
- Scherbatyuk, A. (1995). The AUV positioning using ranges from one transponder LBL. In *Proceedings of the IEEE/MTS OCEANS Conference and Exhibition* (Vol. 3, pp. 1620–1623). Institute of Electrical and Electronics Engineers (IEEE).
- Singh, H., Catipovic, J., Eastwood, R., Freitag, L., Henriksen, H., Hover, F., Yoerger, D., Bellingham, J., & Moran, B. (1996). An integrated approach to multiple AUV communications, navigation and docking. In *Proceedings of the IEEE/MTS OCEANS Conference and Exhibition* (Vol. 1, pp. 59–64). Institute of Electrical and Electronics Engineers (IEEE).
- Singh, S., Grund, M., Bingham, B., Eustice, R., Singh, H., & Freitag, L. (2006). Underwater acoustic navigation with the WHOI micro-modem. In OCEANS 2006 (pp. 1–4). Institute of Electrical and Electronics Engineers (IEEE).
- Smith, R., Self, M., & Cheeseman, P. (1990). Estimating uncertain spatial relationships in robotics. In I. Cox, & G. Wilfong (Eds.), *Autonomous robot vehicles* (pp. 167–193). Springer-Verlag.
- Society of Naval Architects and Marine Engineers (U.S.), Technical and Research Committee, & Hydrodynamics Subcommittee. (1950).

 Nomenclature for treating the motion of a submerged body through a fluid: Report of the American Towing Tank Conference. Technical and research bulletin. Society of Naval Architects and Marine Engineers.
- Song, T. (1999). Observability of target tracking with range-only measurements. *IEEE Journal of Oceanic Engineering*, 24(3), 383–387.
- Spindel, R., Porter, R., Marquet, W., & Durham, J. (1976). A high-resolution pulse-Doppler underwater acoustic navigation system. IEEE Journal of Oceanic Engineering, 1(1), 6–13.

- Teledyne RDI. (2017). Teledyne RD Instruments Explorer Doppler Velocity Log (DVL) Datasheet.
- Thrun, S., Burgard, W., & Fox, D. (2005). Probabilistic robotics, Boston: MIT Press
- Vaganay, J., Baccou, P., & Jouvencel, B. (2000). Homing by acoustic ranging to a single beacon. In *Proceedings of the IEEE/MTS OCEANS* Conference and Exhibition (Vol. 2, pp. 1457–1462).
- Walls, J. M., & Eustice, R. M. (2011). Experimental comparison of synchronous-clock cooperative acoustic navigation algorithms. In *Proceedings of the IEEE/MTS OCEANS Conference and Exhibition* (pp. 1–7). Institute of Electrical and Electronics Engineers (IEEE).
- Walls, J. M., & Eustice, R. M. (2014). An origin state method for communication constrained cooperative localization with robustness to packet loss. The International Journal of Robotics Research, 33(9), 1191–1208.
- Webster, S. E. (2010). Decentralized single-beacon acoustic navigation: Combined communication and navigation for underwater vehicles (Ph. D. thesis). Johns Hopkins University, Baltimore, MD.
- Webster, S. E., Eustice, R. M., Murphy, C., Singh, H., & Whitcomb, L. L. (2009). Toward a platform-independent acoustic communications and navigation system for underwater vehicles. In *Proceedings of the IEEE/MTS OCEANS Conference and Exhibition* (pp. 1–7). Institute of Electrical and Electronics Engineers (IEEE).
- Webster, S. E., Eustice, R. M., Singh, H., & Whitcomb, L. L. (2012). Advances in single-beacon one-way-travel-time acoustic navigation for underwater vehicles. The International Journal of Robotics Research, 31(8), 935–950.
- Webster, S. E., Freitag, L. E., Lee, C. M., & Gobat, J. I. (2015). Towards real-time under-ice acoustic navigation at mesoscale ranges. In 2015 IEEE International Conference on Robotics and Automation (ICRA) (pp. 537–544). Institute of Electrical and Electronics Engineers (IEEE).
- Webster, S. E., Walls, J. M., Whitcomb, L. L., & Eustice, R. M. (2013).
 Decentralized extended information filter for single-beacon cooperative acoustic navigation: Theory and experiments. *IEEE Transactions on Robotics*, 29(4), 957–974.
- Webster, S. E., Whitcomb, L. L., & Eustice, R. M. (2010). Preliminary results in decentralized estimation for single-beacon acoustic underwater navigation. In *Proceedings of the Robotics: Science & Systems Conference*. ISBN 978-0-9923747-4-7. http://www.roboticsproceedings.org/rss14/p34.html
- Whitcomb, L., Yoerger, D., & Singh, H. (1998). Towards precision robotic maneuvering, survey and manipulation in unstructured undersea environments. In *Proceedings of the International Symposium on Robotics Research*. New York: Springer Verlag (pp. 45–54).

How to cite this article: Harris ZJ, Whitcomb LL. Cooperative acoustic navigation of underwater vehicles without a DVL utilizing a dynamic process model: Theory and field evaluation. *J Field Robotics*. 2021;38:700–726.

https://doi.org/10.1002/rob.22008